

AN ANALYSIS OF 12 GHZ LOW ANGLE
RADIOMETRIC DATA

by

Thomas Scott Howard

Thesis submitted to the Faculty of the
Virginia Polytechnic Institute and State University
in partial fulfillment of the requirements for the degree of
MASTER OF SCIENCE
in
Electrical Engineering

APPROVED:

T. Pratt

C. W. Bostian

W. A. Davis

June, 1983
Blacksburg, Virginia

AN ANALYSIS OF 12 GHZ LOW ANGLE RADIOMETRIC DATA

by

Thomas S. Howard

(ABSTRACT)

Several types of radiometers are reviewed for their relative abilities to measure sky noise temperature. Attenuation caused by atmospheric particles (rain, ice, oxygen, etc.) can be predicted from the sky noise temperature. Three years of data (1979-1981) were available for data reduction and analysis. From this data a model is developed to predict attenuation from sky noise temperature. Correlation of the predicted attenuation to actual signal attenuation is performed to assess the validity of the radiometric model.

ACKNOWLEDGEMENTS

I would like to thank my thesis advisor, Dr. T. Pratt, for his support and assistance on this project. I would also like to thank the other members of my committee, Dr. C.W. Bostian and Dr. W.A. Davis for their guidance and suggestions. In addition, I am grateful to Dr. W.L. Stutzman for his help.

I appreciate the help from all the members of the Satellite Communications Group, and I especially wish to thank Kerry Yon, Bob Porter, Claudia Stutzman, Maureen Gaines, and Chip Towner for their efforts in transforming the raw data into a polished form so that it could be analyzed.

Finally, I would like to thank my parents for their constant support throughout undergraduate and graduate school.

TABLE OF CONTENTS

AN ANALYSIS OF 12 GHZ LOW ANGLE RADIOMETRIC DATA ii

ACKNOWLEDGEMENTS iii

Chapter page

I. INTRODUCTION 1

II. TYPES OF RADIOMETERS 3

 Radiometer Theory 3

 Total Power Radiometer 7

 Dicke-Switched Radiometer 10

 Other Radiometers 17

III. VPI & SU RADIOMETER 19

 General Radiometer Specifications 19

 Calibration of the Radiometer 24

 Modeling of the Radiometer System 25

 Radiometer Modeling from Event Analysis 26

 Use of Automatic Calibrations 29

IV. MEDIUM TEMPERATURE 31

 Setting the Medium Temperature 31

 Temperature Analysis of Monthly Data 32

V. RADIOMETRIC EVENTS 53

 Determination of events 53

 Comparison to the Satellite Downlink 54

VI. RADIOMETER PERFORMANCE DURING THE SIRIO EXPERIMENT 72

 Discussion of the Operation of the Radiometer . 72

 Modeling of the Radiometer 73

 Correction Applied to the Events 77

VII. CONCLUSIONS 84

REFERENCES 85

Chapter I

INTRODUCTION

This thesis describes several types of radiometers and discusses their relative advantages and disadvantages. More attention is given to the radiometer types which are used in studies of propagation effects.

The research efforts at the Virginia Polytechnic Institute and State University (VPI & SU) Satellite Communications Group are focused on the propagation of satellite signals through the atmosphere. Rain, snow, ice, clouds and other weather conditions change the characteristics of the satellite signal. Models of the propagation effects of weather can be formulated from long term observations of the signal. A radiometer is often used in conjunction with a satellite receiving station for observing atmospheric effects. The radiometer does not receive the satellite signal; it measures the noise temperature of the atmosphere and from the noise temperature predictions can be made of expected attenuation of the satellite signal.

The VPI & SU Satellite Communications Group conducted a three year experiment (1979 - 1981) observing propagation effects at 11.6 GHz. A 12 GHz radiometer system was used in

this experiment. Data from all three years have been analyzed and the methods and results are contained in this report.

Chapter II

TYPES OF RADIOMETERS

2.1 RADIOMETER THEORY

Radiometers are used to measure noise energy in the electromagnetic spectrum. Noise energy is emitted by the interaction of charged particles in matter at any temperature above absolute zero. If the energy is high enough, the radiation is observable as heat or light. Energy in the radio frequency range is also being emitted and can be detected with an antenna and a radiometer. A simple radiometer model is shown in Figure 2.1-1. It is very similar in design to a communication receiver system. The desired output is the noise power being received at the antenna. The noise power is a maximum when the receiver is conjugate matched to the noise source. For a conjugate match the available noise power is

$$P_N = kTB \quad (2.1.1)$$

where P_N = Available noise power (Watts)

k = Boltzmann's constant (1.38×10^{-23} Joules/Kelvins)

T = Temperature of the noise source (Kelvins)

B = Bandwidth (Hertz)

Noise power and noise temperature can be used interchangeably to describe the noise power available from a

source with a noise temperature, T . Since all matter above 0 K generates noise energy, the receiver section of the radiometer generates a noise power, P_R , equal to

$$P_R = kT_R B_R \quad (2.1.2)$$

where T_R = equivalent noise temperature of the receiver referred to the antenna(K)

B_R = bandwidth of the receiver (Hz)

which adds to the input signal. The noise power at the output of the receiver can be expressed as

$$P_1 = G[kT_R B + k(T_A + \Delta T)B] \quad (2.1.3)$$

where G = Gain of the receiver

T_A = Equivalent noise temperature of the antenna (K)

ΔT = Noise temperature added due to the presence of a noise source (K)

B = Bandwidth of the receiver (Hz)

Rearranging this expression,

$$P_1 = GkB[T_R + (T_A + \Delta T)] = GkBT_1 \quad (2.1.4)$$

The desired signal, ΔT , is contained in the unknown, T_1 , and must be extracted. The voltage at the output of the receiver, V_1 , is fed into the detector. The detector used is often a square law device as given by

$$V_{out} = CV_{in}^2 \quad (2.1.5)$$

The additional noise from the detector is negligible in terms of noise temperature referred to the antenna. The

output of the detector is a voltage proportional to the square of V_1 or

$$V_0 = C_1 V_1^2 = C_1 (kT_1 B_R) \quad (2.1.6)$$

An integrator, usually a simple RC low pass filter, is added after the detector to smooth the random noise fluctuations.

The integrator narrows the bandwidth of the output so that

$$V_0 = C_2 T_1 \quad (2.1.7)$$

where C_2 is the combination of all the constants. The measured noise temperature, T_1 , is proportional to the radiometer output voltage, but is not only the noise source temperature. T_1 also includes the effects of the receiver and background noise. By subtracting a DC voltage from the output voltage the receiver noise temperature can be eliminated.

$$V_0 = CT_1 = C(T_A + \Delta T + T_R) \quad (2.1.8)$$

$$V_{DC} = C(T_A + T_R) \quad (2.1.9)$$

$$V_{out} = V_0 - V_{DC} = C\Delta T \quad (2.1.10)$$

Calibration of the radiometer system allows the proportionality constants to be determined. Any changes in the components in the radiometer requires changing the constants, V_{DC} and C .

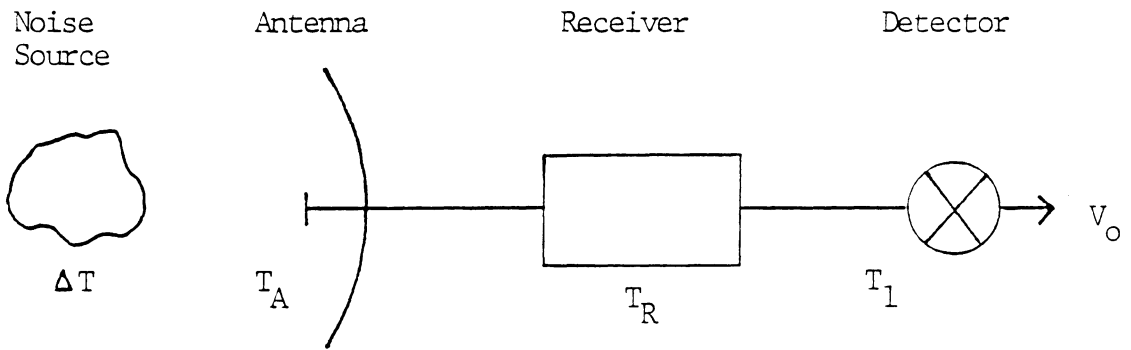


Figure 2.1-1 - Simple Radiometer Model

2.2 TOTAL POWER RADIOMETER

The simplest form of radiometer is the total power radiometer shown in Figure 2.2-1. The RF amplifier is followed by a low noise mixer and a wide band IF amplifier. Without any narrow band filtering before the mixer, the noise at the image frequency band as well as the noise at the signal frequency band is allowed to enter the IF stage. This technique increases the noise power by 3 dB compared to a single side band receiver. Most of the gain (80-100 dB) and selectivity are located in the IF section. A square law detector is used to convert the noise energy to a DC voltage proportional to noise power and the integrator smooths the DC output. Integration time for total power radiometers is typically on the order of tens of seconds. The noise generated by the receiver is usually compensated by an equal -V voltage in the DC amplifier present after the square law detector.[1]

Because the noise signal is very small, the overall gain of the system must be very large. This requires extreme stability in the RF and IF amplifiers.

A useful figure of merit for a radiometer is its temperature sensitivity. Temperature sensitivity is defined as the minimum detectable change in the output signal which can be attributed to a change in the input signal. The

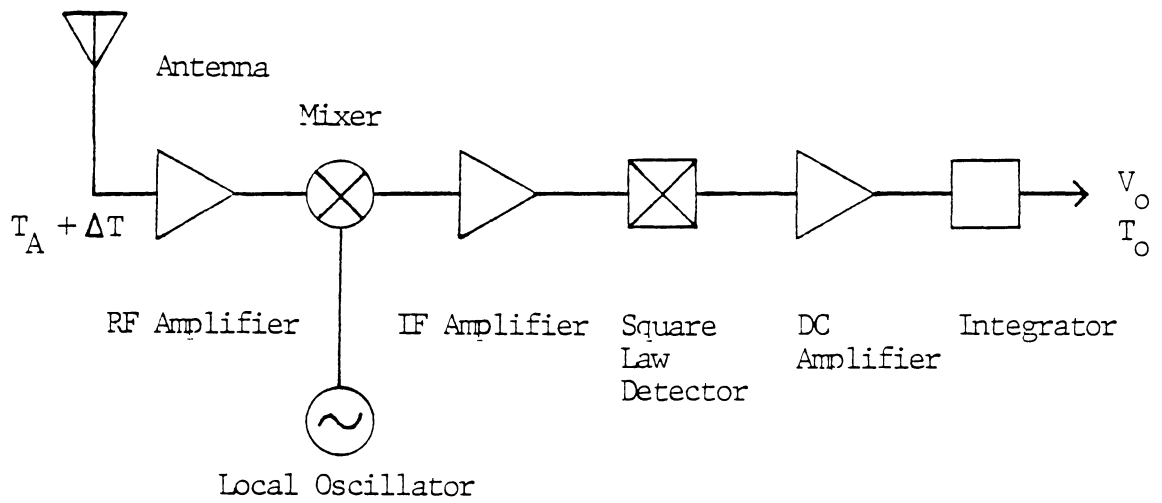


Figure 2.2-1 - Block Diagram of a Total Power Radiometer

receiver cannot distinguish gain fluctuations from changes in the noise signal power. Hence, the sensitivity of this radiometer is limited by its system noise temperature and its gain stability.

The minimum temperature sensitivity is obtained by setting the noise power in the signal equal to the noise power generated by the noise temperature of the system ($T_A + T_R$). Assuming for the moment that the radiometer described above is ideal and exhibits no gain variations, the minimum temperature sensitivity (rms) of the total power radiometer can be expressed as

$$\Delta T_{\min} = T_{SN} (2B_{LF}/B_{HF})^{\frac{1}{2}} \quad (2.2.1)$$

where $T_{SN} = T_A + T_R =$ Antenna noise temperature + receiver noise temperature

$B_{LF} =$ Output bandwidth

$B_{HF} =$ Predetection bandwidth

A complete development of equation (2.2.1) can be found in [1]. If the detector output is taken to an ideal integrator which averages the signal over τ seconds then,

$$B_{LF} = 1/(2\tau) \quad (2.2.2)$$

and the minimum temperature sensitivity is then

$$\Delta T_{\min} = T_{SN} / (B\tau)^{\frac{1}{2}} \quad (2.2.3)$$

In a practical radiometer, small gain variations modify the minimum temperature sensitivity to

$$\Delta T_{\min} = T_{SN} [1/B\tau + (\Delta G/G)^2]^{\frac{1}{2}} \quad (2.2.4)$$

where ΔG = rms gain fluctuations

G = average gain of the entire system

For a radiometer with a system noise temperature, $T_{SN} = 1000$ K, a bandwidth, $B = 100$ MHz, and an integration time, $\tau = 10$ sec, the minimum temperature sensitivity from equation (2.2.3) is 0.03 K. However gain changes can easily degrade this figure. A gain fluctuation of only 0.1 dB out of 100 dB of total gain drastically affects the temperature sensitivity : using the same values quoted above and equation (2.2.4) yields a temperature sensitivity of 23 K. The total power radiometer is gain fluctuation limited rather than noise limited.

2.3 DICKE-SWITCHED RADIOMETER

Many schemes have been devised to overcome the gain instability problem. This section describes the types of Dicke-switched Radiometers. The basic form of this radiometer was first described by R. H. Dicke in [3]. The Dicke radiometer as shown in Figure 2.3-1 includes a pulse generator, an RF switch (usually ferrite or a semiconductor diode), and a synchronous detector. The switch connects the radiometer input alternately to the antenna and a stable temperature source, T_{ref} . The switching frequency is usually between 10 and 1000 Hertz and during one cycle the gain of

the radiometer is assumed to remain constant. During the period that the receiver is connected to the antenna the output voltage after the synchronous detector is

$$V_A = C_1 G k (T_A + T_R) B \quad (2.3.1)$$

where C_1 , G = gain constants of the receiver

k = Boltzmann's constant

B = Effective bandwidth of receiver (Hz)

T_A = Antenna noise temperature (K)

T_R = Receiver noise temperature (K)

The output when the switch is in the reference position is

$$V_{ref} = C_1 G k (T_{ref} + T_R) B \quad (2.3.2)$$

The final DC output after synchronous detection will be proportional to the difference between these voltages

$$V_{out} = C_2 (V_A - V_{ref}) = C_1 C_2 G k (T_A - T_{ref}) B \quad (2.3.3)$$

In terms of noise temperatures

$$\Delta T = (T_A - T_{ref}) \Delta G / G \quad (2.3.4)$$

Clearly if the antenna temperature, T_A , equals the reference temperature, T_{ref} , any gain fluctuations, ΔG , will not affect the output. The receiver sensitivity is then limited only by the system noise performance.[1] For a Dicke-switched radiometer with square wave modulation the receiver is connected to the antenna only half of the time and therefore the minimum temperature sensitivity is only one half of the theoretical sensitivity of the total power radiometer (equation 2.2.3) or

$$\Delta T_{\min} = 2T_{\text{SN}}/(B\tau)^{\frac{1}{2}} \quad (2.3.5)$$

The amplifier following the square law detector must have a bandwidth wide enough to pass several harmonics of the square-wave modulated signal. One alternative to using a wide bandwidth amplifier is to use a sine wave input to the synchronous detector and a narrow bandpass filter to pass only the fundamental frequency. This allows for simpler narrowband amplifiers but decreases the sensitivity by 10 percent or

$$\Delta T_{\min} = \pi T_{\text{SN}}/(2B\tau)^{\frac{1}{2}} = 2.22T_{\text{SN}}/(B\tau)^{\frac{1}{2}} \quad (2.3.6)$$

These sensitivities assume a balanced condition of $T_A = T_{\text{ref}}$ in equation (2.3.4). An attenuator placed in the temperature reference arm can be adjusted to set T_{ref} equal to T_A . One variation on a Dicke-switched radiometer can easily obtain a balanced condition [4]. The gain-modulated Dicke-switched radiometer of Figure 2.3-2 includes a preset attenuator and a variable attenuator in the IF section. The gain of the system is G_A when the switch connects the radiometer to the antenna and G_{ref} when the switch is turned to the reference temperature. For a balanced condition

$$(T_A + T_R)G_A = (T_{\text{ref}} + T_R)G_{\text{ref}} \quad (2.3.7)$$

Achieving a balanced system is done during a calibration by adding or subtracting attenuation in the IF amplifier until a null at the output is achieved. The balanced condition is

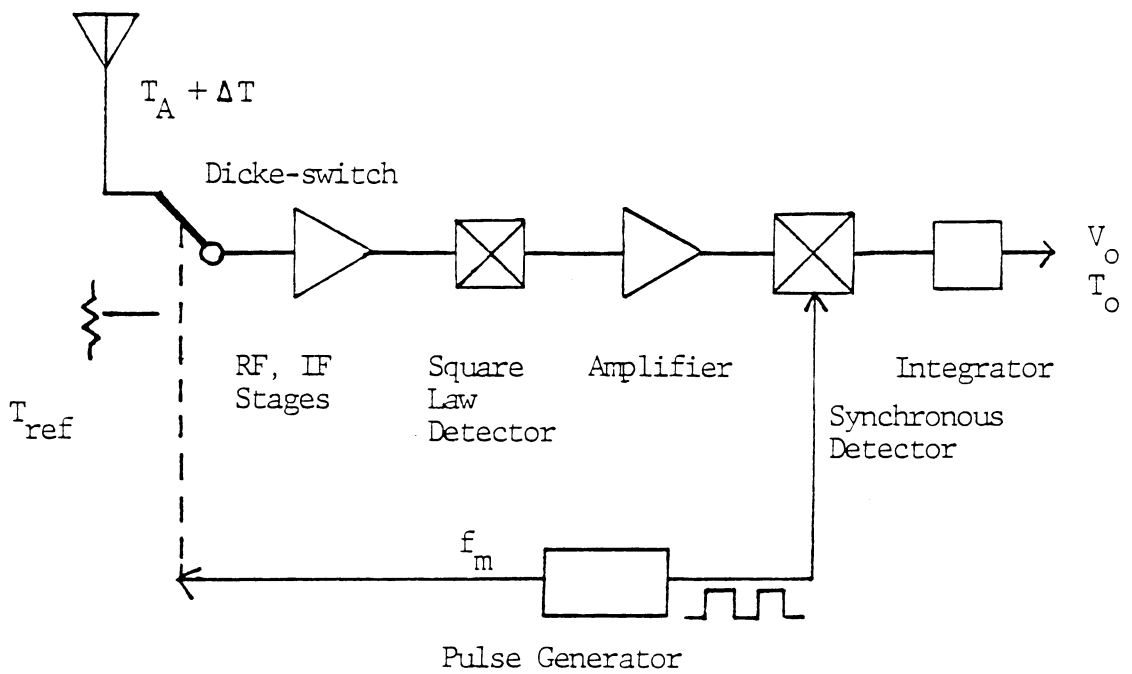


Figure 2.3-1 - Block Diagram of a Simple Dicke-Switched Radiometer

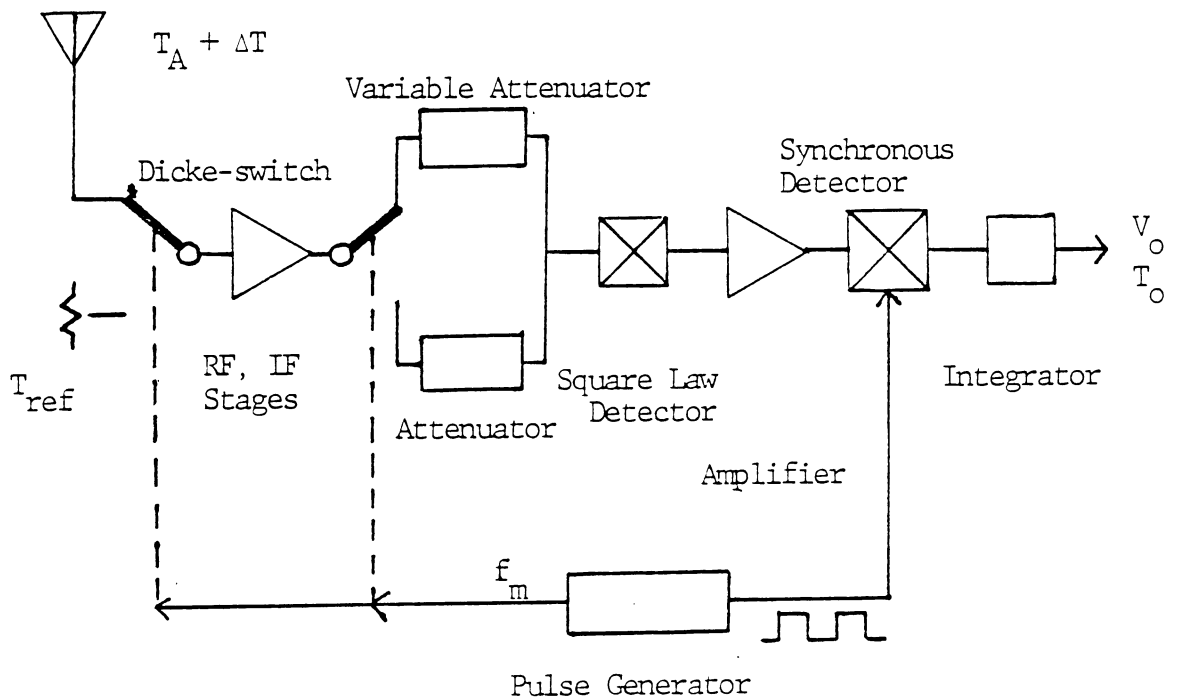


Figure 2.3-2 - Block Diagram of a Gain Modulated Dicke-Switched Radiometer

upset in the presence of a signal and the radiometer will be susceptible to gain fluctuations when a signal is present. These possible fluctuations serve to limit the minimum temperature sensitivity of the receiver. A third variation of the Dicke radiometer overcomes this problem by maintaining a balanced condition even in the presence of a signal. The null-balancing Dicke-switched radiometer (Figure 2.3-3) feeds the output of the integrator through a controller which adjusts the noise source to exactly match the antenna temperature. The output is the voltage being fed to the noise source.

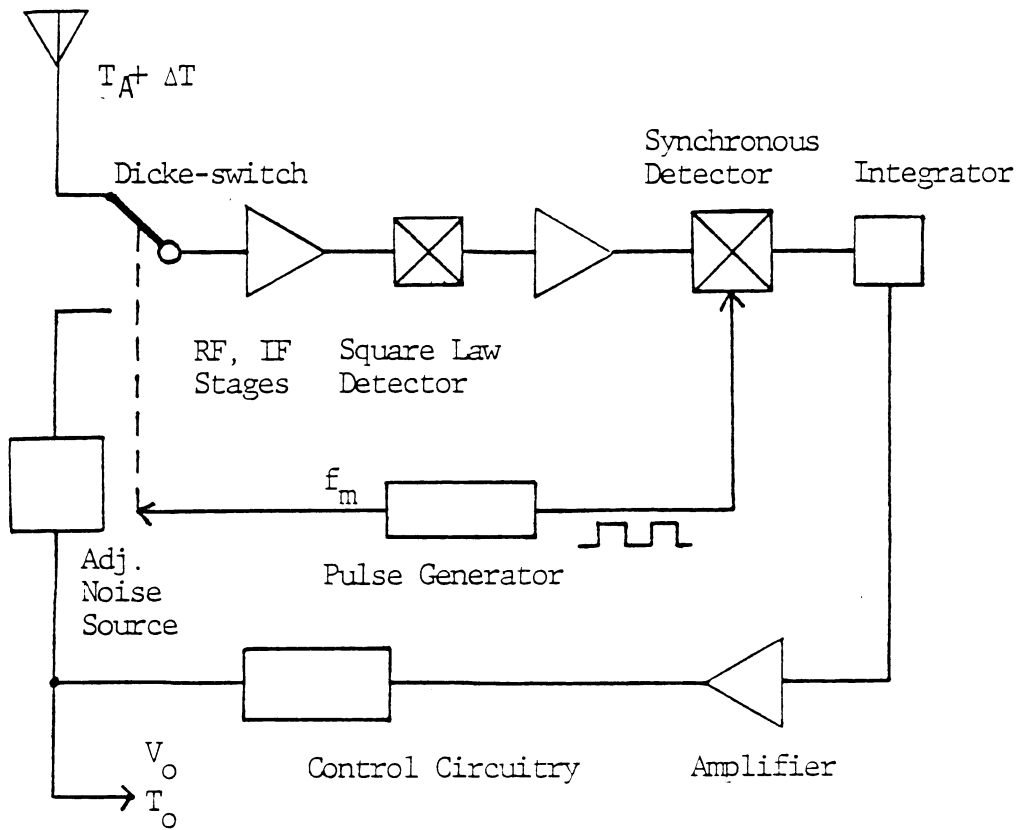


Figure 2.3-3 - Block Diagram of a Null-Balancing Dicke-switched Radiometer

2.4 OTHER RADIOMETERS

Many other variations on the basic radiometer design have been developed. This section briefly discusses some of them.[2,5] Graham's radiometer combines two front end sections of the radiometer so that one is attached to the antenna while the other is attached to a reference temperature source. The output of each is added out of phase to increase the overall sensitivity of the system.

The correlation radiometer uses two RF and IF sections coupled to the same antenna. Their outputs are then combined so that correlated signals (i.e. from the antenna) produce a DC output. The noise voltages produced by the two receivers are uncorrelated and therefore will on average yield a zero output voltage. Care must be taken to prevent noise from one receiver from entering the other receiver and giving a partially correlated output.

The phase-switching radiometer uses two antennas and two RF and IF sections. The IF outputs are added in phase and then out of phase at a modulating frequency, f_m . When the IF outputs contain correlated components the addition of the two signals is different from the subtraction of the two signals. After synchronous detection only the proportional difference remains and can be directly related to the antenna temperature. The sensitivity of this system is the same as the simpler Dicke switched radiometer.

All radiometers must be calibrated to convert the output voltage to the source noise temperature. By subjecting the antenna to a radiation with a known noise temperature and then recording the output voltage, one noise temperature point is known. A second calibrated noise source placed over the antenna feed will cause a different output voltage. Assuming linearity in all stages of the radiometer (excepting, of course, the square law detector) the slope in Kelvins/volt can be determined.

Chapter III

VPI & SU RADIOMETER

The radiometer used for collecting data at the VPI & SU Satellite Tracking Station was co-located with a 11.6 GHz receiver and 12 foot fully steerable parabolic antenna. The receiver was used to measure the signal level of a 11.6 GHz beacon located on the SIRIO satellite in geosynchronous orbit. The antenna was pointed at an elevation angle of 10.7 degrees and an azimuth of 105 degrees. The receiver measures the beacon or copolar signal, and also the orthogonal channel, or crosspolar signal. The radiometer antenna was positioned approximately 20 meters away from the main antenna, and was pointed along the same downlink path as the SIRIO satellite.

3.1 GENERAL RADIOMETER SPECIFICATIONS

The radiometer at the Satellite Tracking Station was an AIL Type 2392C Universal Radiometer. This unit contained only the IF section of the radiometer. Located directly behind the 6 foot antenna was the radiometer RF stage which contained a 12 GHz Gunn diode local oscillator, an RF latching ferrite switch, switching circuitry, an IF amplifier and the reference noise temperature source (Figure 3.1-1).

The IF signal was transmitted through coaxial cable to the Tracking Station and the Universal Radiometer (so called because it allows many modes of operation.) The radiometer provided a total power output, or it could be used as a Dicke-switched radiometer. Another switch allows it to operate as a gain modulated Dicke-switched radiometer (See Figure 2.3-2). It was in this mode that the radiometer was operated during the three year experiment.

During calibration of the radiometer a balanced condition was set up to make the radiometer insensitive to gain changes. In the presence of a signal at the antenna the sensitivity would be decreased only when short-term gain changes occur. The temperature change due to gain fluctuation was [6]

$$\Delta T_g = [(T_A + T_R)G_A - (T_{ref} + T_R)G_{ref}]\Delta G/G \quad (3.1.1)$$

where T_A = antenna temperature

T_R = Receiver noise temperature

T_{ref} = Reference load temperature

G_{ref} = IF gain when system is connected to the
reference, T_{ref}

G_A = IF gain when system is connected to the
antenna, T_A

ΔG = gain variations (rms)

G = average gain of the IF stage

Then, if

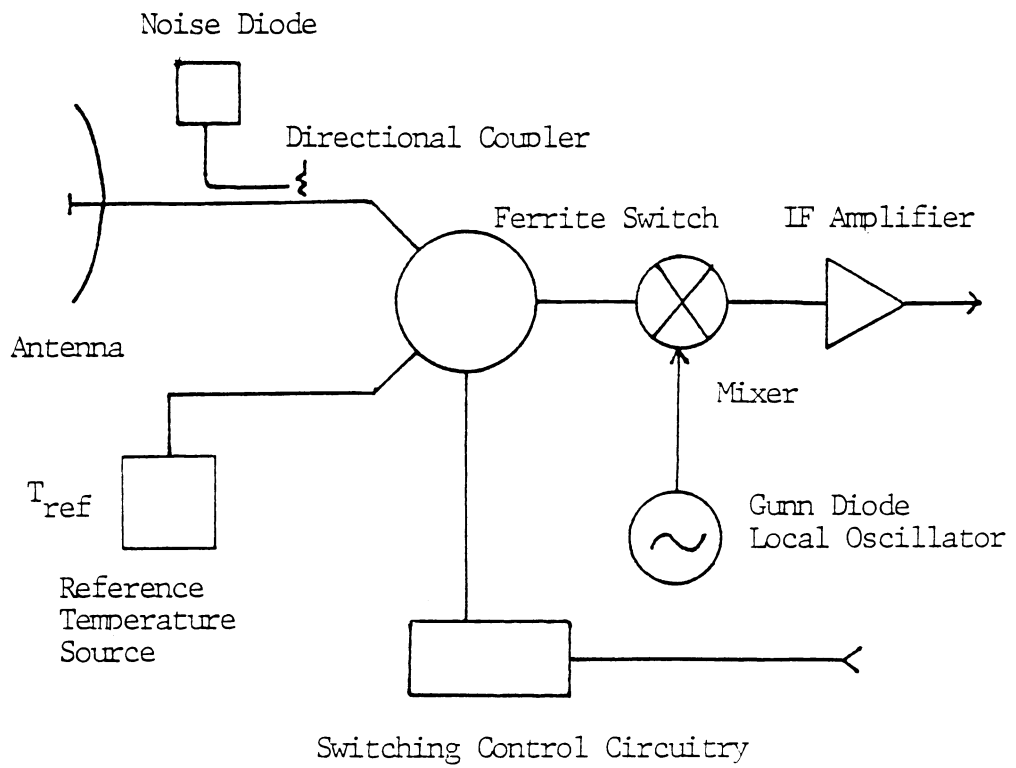


Figure 3.1-1 - VPI & SU Radiometer RF Section

$$G_{\text{ref}}/G_A = (T_A + T_R)/(T_{\text{ref}} + T_R) \quad (3.1.2)$$

$\Delta T_g = 0$ and the receiver was balanced. When a signal was present, the antenna temperature, T_A , became $T_A + \Delta T$. Using similar values to the example in section 2.2, $T_R = 1000$ K, $T_A = 100$ K, $\Delta G = 0.1$ dB, $G = 100$ dB, and using $T_{\text{ref}} = 343$ K and $\Delta T = 150$ K yields from equation (3.1.2)

$$G_{\text{ref}}/G_A = 0.8316$$

Substituting into equation (3.1.1) gives a $\Delta T_g = 3.5$ K which is much better than the 23 K previously calculated for a gain change of 0.1 dB but no gain modulation scheme.

Other features of this radiometer are switchable integration time constants, a variable frequency oscillator for the RF switch rate, IF gain modulation and synchronous detector, and variable IF GAIN. A phase adjust knob was also provided to compensate for time delays between the Dicke switch and the synchronous detector. The synchronous detector was essentially a switch which reversed its polarity in synchronism with the RF (Dicke) switch. This switching action rectified the modulated waveform. Random noise, which was the input signal, was unaffected by the rectification but the modulation of the signal became a DC offset voltage. [5] Smoothing of the detector output was accomplished with a simple adjustable RC integrator. The values used for the radiometer experiment are listed in Table 3-1.

Table 3-1 - Operating Characteristics of the VPI & SU Radiometer System

Type	Dicke-Switched, gain modulated
Antenna	
Diameter	6 foot
Gain	45.4 dB
Beamwidth	0.8 degrees
IF Amplifier	
Bandwidth	100 MHz
Noise Figure	7 dB
Gain	72 dB out of 85 dB max.
Modulator	Latching ferrite switch
Modulation Frequency	383 Hz (square wave)
Output Voltage	+5 to -5 volts
Time Constant	3 seconds

3.2 CALIBRATION OF THE RADIOMETER

Two methods of calibrating the radiometer were used. The manual calibration was supposed to be performed once every two weeks. This calibration procedure was necessary to convert the deflection of the chart recorder pen (in inches) into Kelvins. The manual calibrations were performed during clear weather. Liquid nitrogen (N_2 , 80 °K) was used for the 'cold' temperature source. The liquid nitrogen was poured into a tin can which was lined with thermal insulation and microwave absorbant material. After the temperature stabilized, the can was placed over the feed of the radiometer antenna. The output of the radiometer was being recorded on a strip chart and the deflection caused by the cold temperature source was marked 'COLD LOAD'. A 'hot' load, usually at ambient temperature (280 - 290 °K) was similarly placed on the antenna feed. The pen deflection caused by this temperature source was marked 'HOT LOAD'. From these two points the slope in Kelvins per inch was calculated. The reference load at 343 K was used as the most accurate temperature point and from the point-slope formula

$$T_{out} = 343 - \text{slope} * (H_{ref} - H_{sig}) \quad (3.2.1)$$

where H_{ref} = Height of the reference temperature
point (inches)

H_{sig} = Height of the signal (inches)

slope = Slope found during manual calibration
(Kelvins/inch)

the temperature of the signal was determined.

During normal operation of the radiometer, an automatic check was performed. The radiometer switched once an hour to the reference temperature load (for about 2 minutes) and then it turned on a noise diode which, through an attenuator and waveguide directional coupler, coupled to the RF input. The diode added approximately 150 K of noise to the signal. These were both tested during a manual calibration and their output (pen deflection in inches) was recorded. The operational status of the radiometer can be detected by examination of these reference points. The reference temperature (assumed constant at 343 K) point, H_{ref} , can be determined at the time of an event (presence of a signal) for greatest accuracy.

3.3 MODELING OF THE RADIOMETER SYSTEM

The radiometer system to be modeled includes the antenna, RF, IF, and integration sections. At the output of the integration section a voltage is produced which is proportional to the antenna noise temperature. During calibration, various noise sources are placed over the antenna feed to determine the slope (K/inch) of the

calibration curve. However, the antenna noise temperature is not the desired result. In this experiment the noise temperature of the sky is the desired quantity. The antenna noise temperature includes the noise received by the sidelobes and residual noise generated by the antenna. The sidelobes look at a different portion of the sky than the main beam and allow some unwanted noise energy to enter the radiometer. The largest contribution of noise comes from the sidelobes which are directed at the ground. The ground has a much higher noise temperature than the usually cold sky and will add significantly to the apparent received noise temperature. A model of the radiometer system is required which allows the sky noise temperature to be extracted from the measured antenna noise temperature data.

3.4 RADIOMETER MODELING FROM EVENT ANALYSIS

Construction of a simple radiometer system model allows the true sky noise temperature to be determined. Figure 3.4-1 shows the model, where α is the antenna transfer efficiency and T_e is a source of additional antenna noise. The noise temperature measured at the radiometer detector output is T_o and T_{sky} is the noise temperature of that part of the sky which fills the ideal antenna main beam (i.e. no sidelobes). T_{sky} is the desired temperature and is the same

quantity as ΔT discussed in Chapter II. The measured output is then

$$T_o = \alpha T_{\text{sky}} + T_e \quad (3.4.1)$$

From calibration of the radiometer with a 'hot load' noise source at 343 K, the recorded noise temperature, T_o , at any point on a strip chart recorder can be determined. Two more reference points are necessary to determine values for α and T_e . One obvious point is the noise temperature of a cold, clear sky, T_{CS} . From [7], the noise temperature of the sky in clear air at an elevation angle of 10.7 degrees, a frequency of 12 GHz, an ambient temperature of 0 °C and with a water content of 3 gm/m³, T_{CS} is 20 K. From a careful analysis of periods of clear weather in December, January, and February of 1979 and 1980, the average minimum recorded temperature was 35 K. Therefore, in cold clear weather periods

$$35 = \alpha(20) + T_e \quad (3.4.2)$$

The second reference point is not nearly so obvious. A hot reference temperature point is needed. One distinct temperature value cannot be found; it is necessary to assume a maximum temperature. In this experiment when intense rainfall completely fills the antenna beam the sky temperature will approach a maximum value. This value is the medium temperature and is used later in the analysis to

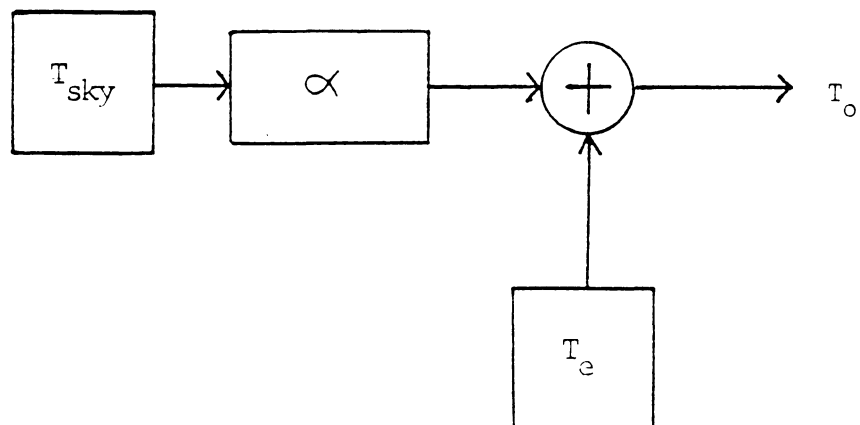


Figure 3.4-1 - Radiometer Model for Determining Sky Noise Temperature, T_{sky} , from Radiometer Output Noise Temperature, T_o

calculate rain - induced attenuation from sky temperature. The assumption made here of $T_m = 265$ K will be checked later for its accuracy in predicting attenuation. A discussion of how this value was chosen can be found in Chapter IV. Analyzing many events in the months of June, July and August of 1979 and 1980, an average maximum temperature $T_{hs} = 270$ K was determined. The hot sky noise temperature equation is then

$$270 = \alpha(265) + T_e \quad (3.4.3)$$

Solving equations (3.4.2) and (3.4.3) gives

$$\alpha = 0.96 \text{ and } T_e = 15.8 \text{ K} \quad (3.4.4)$$

The sky temperature from equation (3.4.1) is

$$T_o = .96T_{sky} + 15.8 \quad (3.4.5)$$

or

$$T_{sky} = 1.04T_o - 16.46 \quad (3.4.6)$$

This is the equation used to convert the recorded output noise temperature, T_o , to the actual sky noise temperature, T_{sky} .

3.5 USE OF AUTOMATIC CALIBRATIONS

The Type 2392C Universal Radiometer performed two automatic checks on itself each hour. First, the radiometer switched to the reference noise temperature source (343 K) and then, approximately five minutes later it switched on a

noise diode which was directionally coupled to the input waveguide. Approximately 150 K was added to the signal noise temperature. During analysis of the radiometer output both of these signals are used. The height of the reference noise temperature points (one per hour) are averaged over the entire length of an event (Events are periods of time when significant changes in the radiometer output are observed). The average height obtained is used as the starting point in the analysis. This is H_{ref} in equation (3.2.1). The added noise temperature provided by the noise diode is not used in the direct analysis of the events but can be used to detect problems with the radiometer. The height (in inches) that the noise diode adds to the signal at the output of the radiometer was recorded each time the radiometer was manually calibrated. If the noise diode additive noise temperature exhibits a drastic change during an event compared to the last manual calibration value the radiometer was probably malfunctioning. Large differences between the value found during a manual calibration and the average value found during the event indicate some form of gain change occurred outside the gain modulated control loop. Chapter VI explores the problem in greater depth.

Chapter IV

MEDIUM TEMPERATURE

4.1 SETTING THE MEDIUM TEMPERATURE

Radiometer output is expressed as a sky noise temperature in Kelvins. For data which can be compared to the beacon signal the noise temperature must be converted to an attenuation value. Assume that the atmosphere is a uniform, lossy medium with a loss, L (greater than 1), and a physical temperature, T_m . This is a partially absorbing medium and will have an equivalent black-body temperature given by [8]

$$T_b = T_a/L + T_m(1 - 1/L) \quad (4.1.1)$$

where T_b = Black-body temperature (K)

T_a = Temperature beyond atmosphere (K)

T_m = Uniform temperature of the atmosphere (K)

L = Loss

The temperature of free space, T_a , is practically zero so equation (4.1.1) becomes

$$T_{sky} = T_m(1 - 1/L) \quad (4.1.2)$$

where T_{sky} has replaced the black-body temperature. Solving for the loss,

$$L = T_m/(T_m - T_{sky}) \quad (4.1.3)$$

Expressed as attenuation, A , in dB,

$$A = 10\log[T_m/(T_m - T_{sky})] \quad (4.1.4)$$

The expression used for converting sky noise temperature to attenuation is

$$A = -10\log[(T_m - T_{sky})/T_m] + \Delta \quad (4.1.5)$$

where Δ = Offset level (dB)

The medium temperature, T_m , is the determining factor in equation (4.1.5) but the medium temperature doesn't have to equal the physical sky temperature. This temperature is determined from analysis of the events and, from a search of the literature on radiometer calibration, [9,10,11,12,13] was assumed to be 265 K. This temperature takes into account the noise power received by the antenna sidelobes, the differences in the beamwidths of the radiometer antenna and the satellite antenna, and other effects such as scintillation of the signal. The offset, Δ , includes two terms, a zero-level attenuation due to the fact that attenuation on the copolar link was set relative to an arbitrary reference level and a low-frequency drift in the attenuation zero level. [10]

4.2 TEMPERATURE ANALYSIS OF MONTHLY DATA

Shown in figures 4.2-1 through 4.2-8 are scatter plots of the radiometer sky noise temperature versus the attenuation ratio of the copolar link for representative months in 1979, 1980, and 1981. All valid data points between 0 dB and 15 dB

of beacon attenuation are plotted but for the linear regression analysis only the data points between 3 dB and 15 dB are included. Below 3 dB the offset, Δ , causes uncertainty in the radiometer predicted attenuation and above 15 dB equation (4.1.5) is very sensitive to small changes in the sky noise temperature. By plotting the noise temperature versus the ratio of attenuation, to a first approximation the points lie along a straight line. The x-intercept corresponds to infinite attenuation, or from equation (4.1.5), $T_{\text{sky}} = T_m$. The y-intercept is the offset level expressed as a ratio.

These six months exhibit a spread of values for both Δ and T_m . The correlation coefficient for a month of data varies from -0.3 to -0.75. Some months, such as February 1979 and January, 1980, show good correlation between 3 and 15 dB. Other months are not nearly as well correlated. The partial correlation is due to two effects and it is difficult to separate one from the other. The radiometer is not expected to have perfect correlation to the beacon attenuation. The two systems have different antenna beamwidths and therefore as rain or other weather conditions move through the downlink path they affect the radiometer and the beacon signal differently. Also, during periods of intense rain the recorded sky noise temperature will reach a

maximum; ideally this value would always be the medium temperature. The dynamic range of the radiometer given this saturation point is about 15 dB. The dynamic range of the satellite receiver is close to 40 dB. The second correlation problem is one of time correlation between the two signals. Both signals (radiometer noise temperature and copolar attenuation) were digitized from the same chart but differences between the absolute time of the two signals can and did occur. This difference could reach three minutes and a quick attenuation spike lasting only a minute at a high attenuation level would be uncorrelated with the radiometer noise temperature spike. May 1979 shows this problem; it contains data points of varying copolar attenuation for high values of sky noise temperature and varying sky noise temperature for high attenuation values.

Months such as February 1979 with only low values of attenuation (no points exceed 7 dB) usually yield a lower value for the medium temperature. During months which contain large attenuation events, such as May 1979 and April 1980, the medium temperature calculated by the linear regression will be higher. The average medium temperature derived from the linear regression analysis for 11 months in 1979 (December contained no values greater than 3 dB) is 271 K and the offset is 0.4 dB. The average medium temperature

calculated in 1980 (11 months - December contained too few points for analysis) is 270 K with an offset of 1.0 dB. For 1981, the average medium temperature is 266 K with an offset of 1.6 dB. The values are very close to 265 K and this justifies the use of a medium temperature of 265 K for predicting the attenuation. Figures 4.2.9 through 4.2.16 show the same months as scatter plots of copolar attenuation (CO) versus radiometer predicted attenuation (RAD). These plots used a medium temperature of 265 K but did not include the effects of the offset value. The radiometer attenuation therefore has a minimum attenuation of 0.3 to 0.7 dB depending on the month. This offset is variable but for values around 0.5 dB this attenuation is chiefly caused by water and oxygen molecules in the air. From [7, Figure 3] the attenuation due to these molecules (principally oxygen) is 0.007 dB/km. The radiometer has an elevation angle of 10.7 degrees and from [7, Figure 1] the equivalent atmospheric thickness from ground level is eight kilometers. The density of the atmosphere decreases exponentially with altitude. The slant-path length through the atmosphere is then 43 kilometers for a total attenuation of 0.3 dB. During periods of high humidity the offset could reach 0.6 dB. The analysis of the radiometer events will initially be made with the offset level set to zero. Later the effects

of adding the offset to the beacon attenuation will be examined.

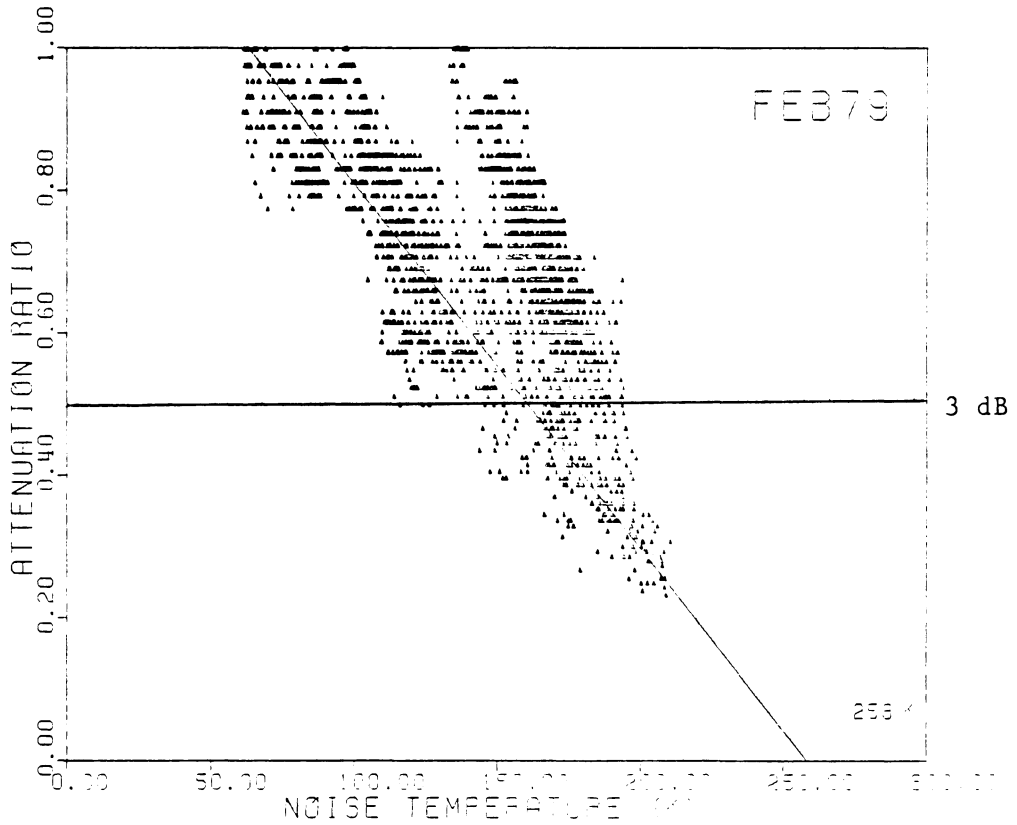


Figure 4.2-1 - Scatter Plot of Beacon Attenuation Ratio versus Sky Noise Temperature for February 1979, at 12 GHz, 10.7 degrees elevation angle, Blacksburg, VA (Linear regression applied only to points below line)

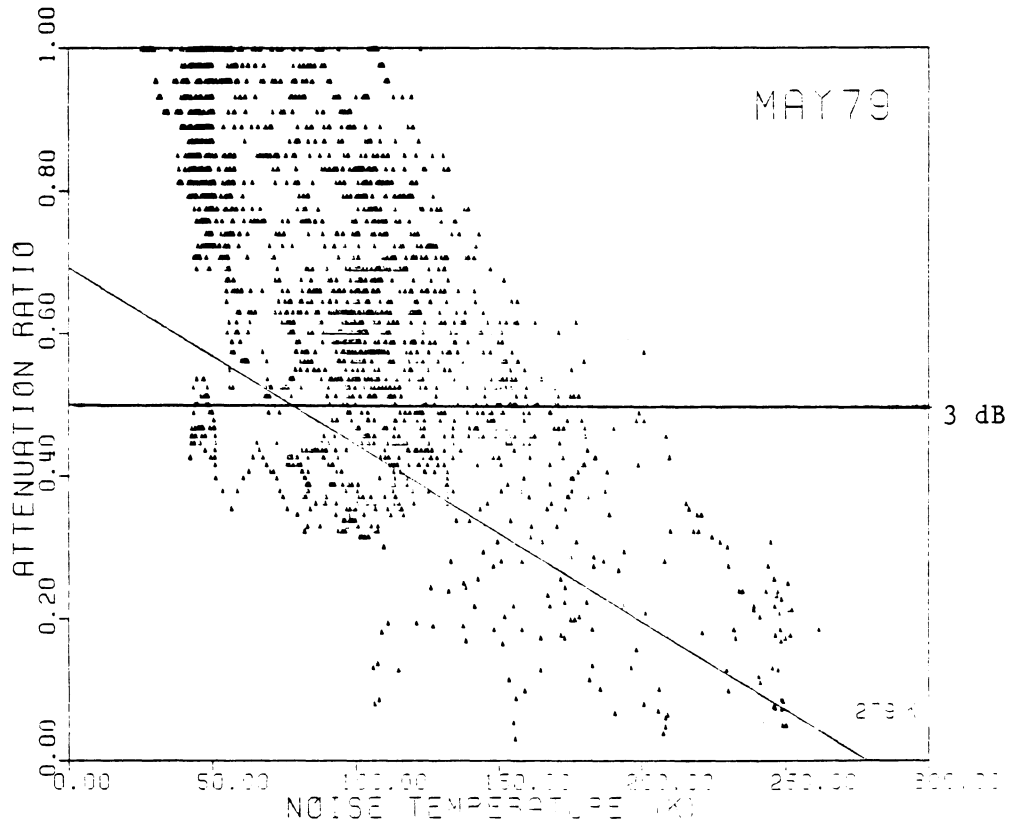


Figure 4.2-2 - Scatter Plot of Beacon Attenuation Ratio versus Sky Noise Temperature for May 1979, at 12 GHz, 10.7 degrees elevation angle, Blacksburg, VA (Linear regression applied only to points below line)

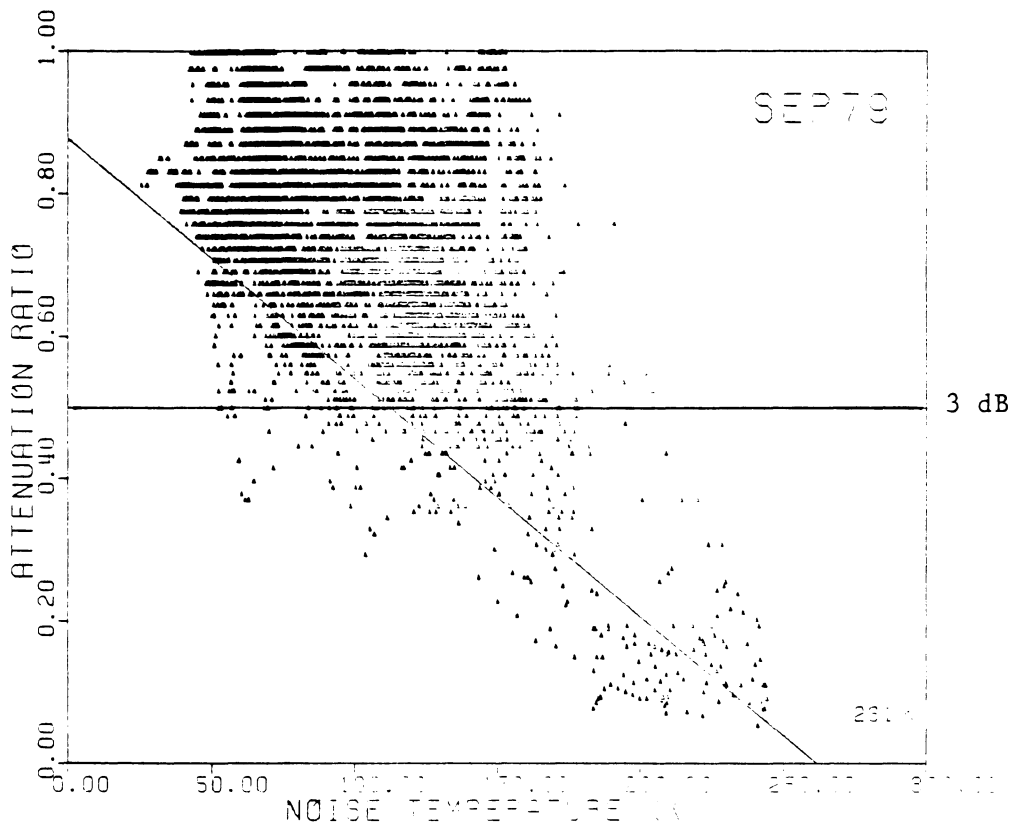


Figure 4.2-3 - Scatter Plot of Beacon Attenuation Ratio versus Sky Noise Temperature for September 1979, at 12 GHz, 10.7 degrees elevation angle, Blacksburg, VA (Linear regression applied only to points below line)

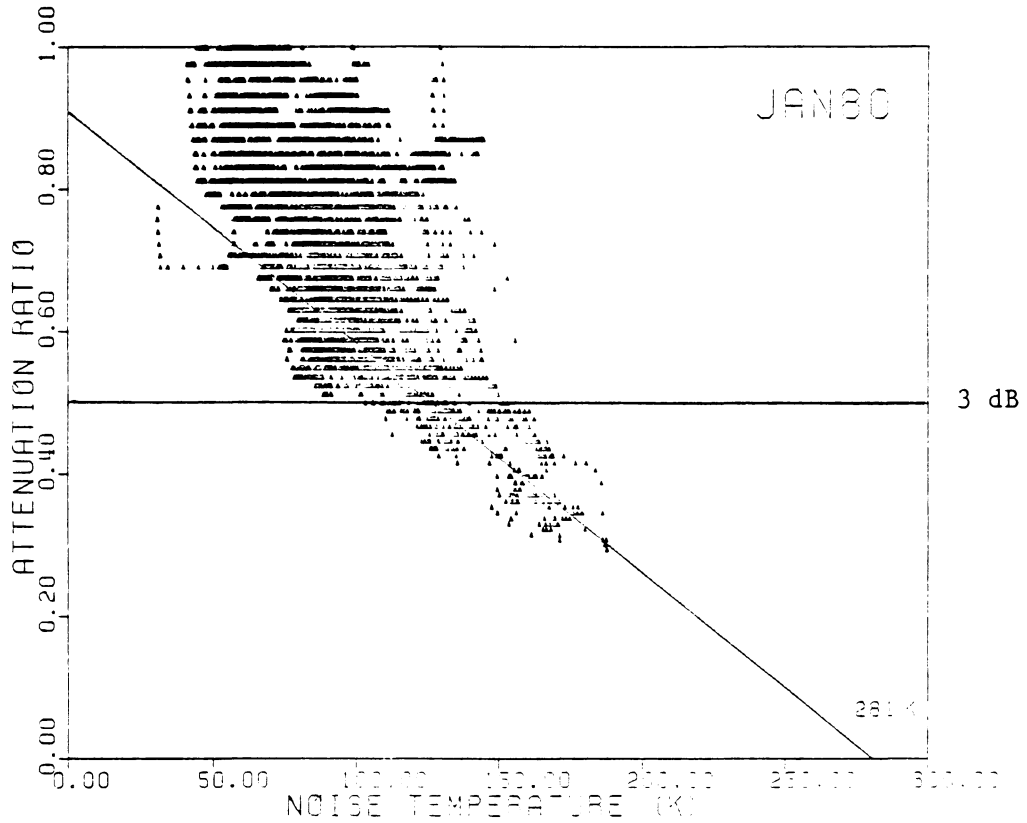


Figure 4.2-4 - Scatter Plot of Beacon Attenuation Ratio versus Sky Noise Temperature for January 1980, at 12 GHz, 10.7 degrees elevation angle, Blacksburg, VA (Linear regression applied only to points below line)

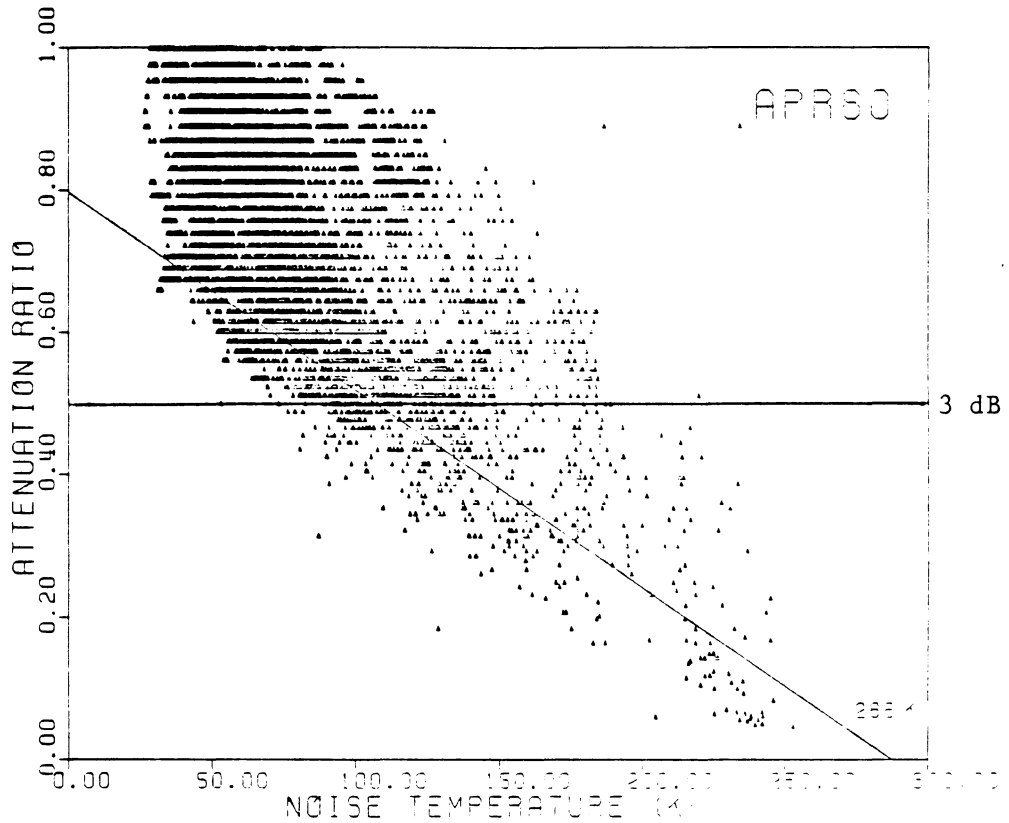


Figure 4.2-5 - Scatter Plot of Beacon Attenuation Ratio versus Sky Noise Temperature for April 1980, at 12 GHz, 10.7 degrees elevation angle, Blacksburg, VA (Linear regression applied only to points below line)

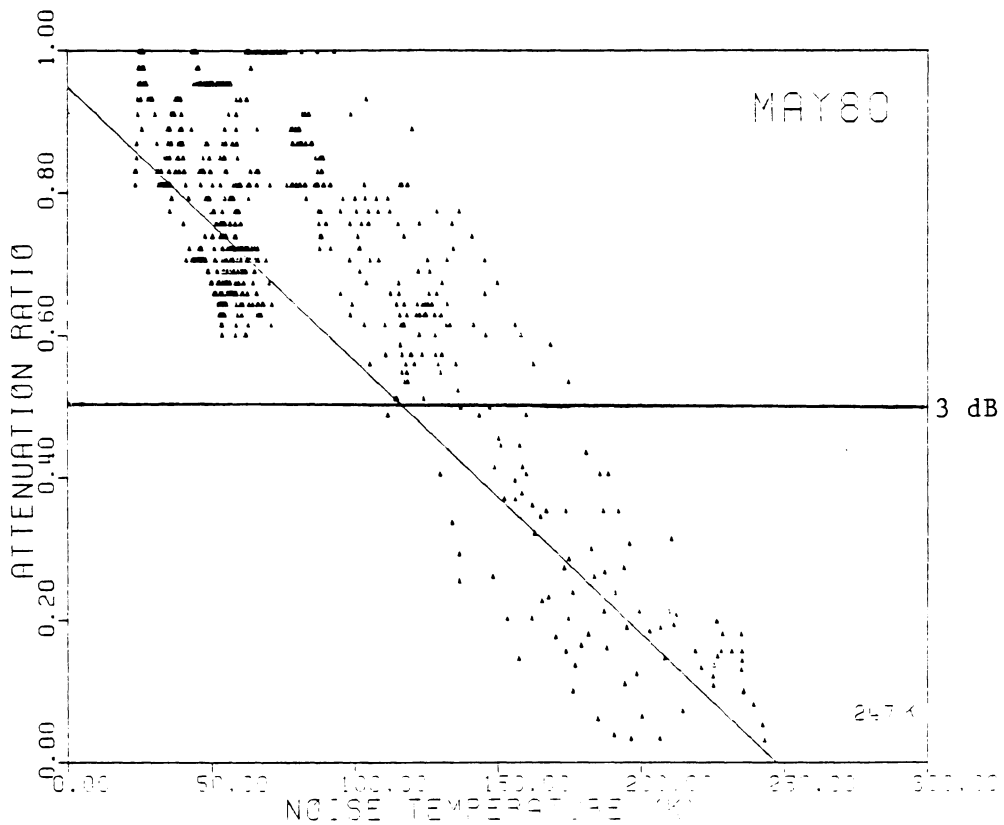


Figure 4.2-6 - Scatter Plot of Beacon Attenuation Ratio versus Sky Noise Temperature for May 1980, at 12 GHz, 10.7 degrees elevation angle, Blacksburg, VA (Linear regression applied only to points below line)

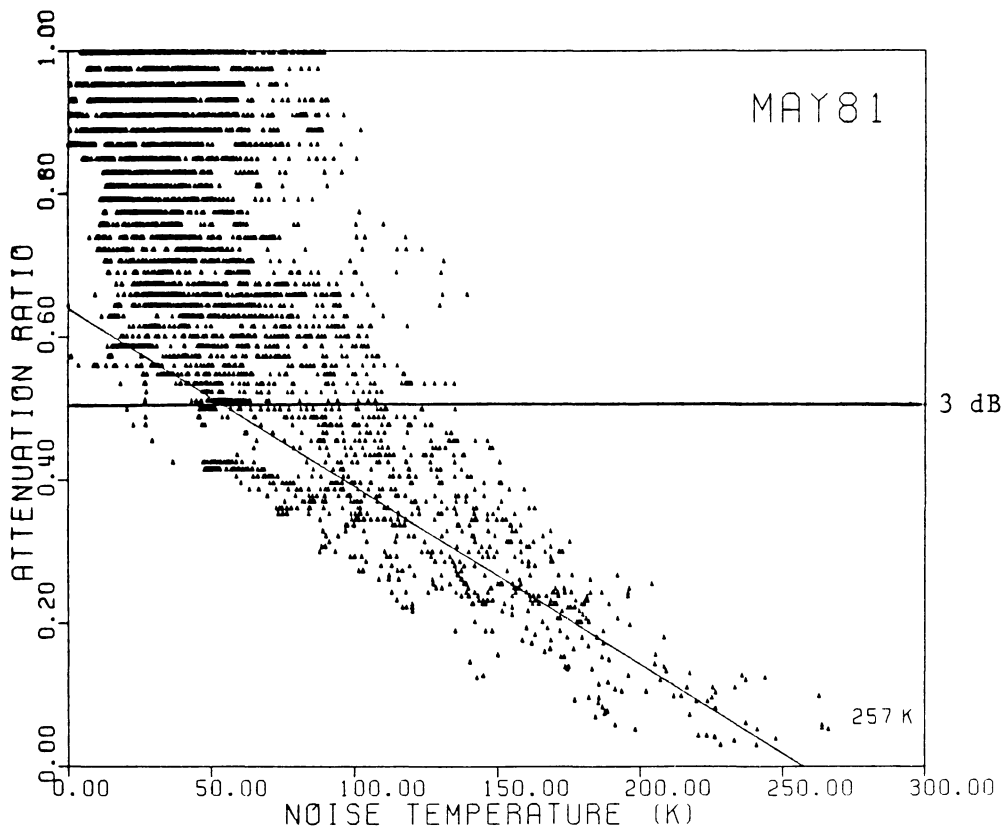


Figure 4.2-7 - Scatter Plot of Beacon Attenuation Ratio versus Sky Noise Temperature for May 1981, at 12 GHz, 10.7 degrees elevation angle, Blacksburg, VA (Linear regression applied only to points below line)

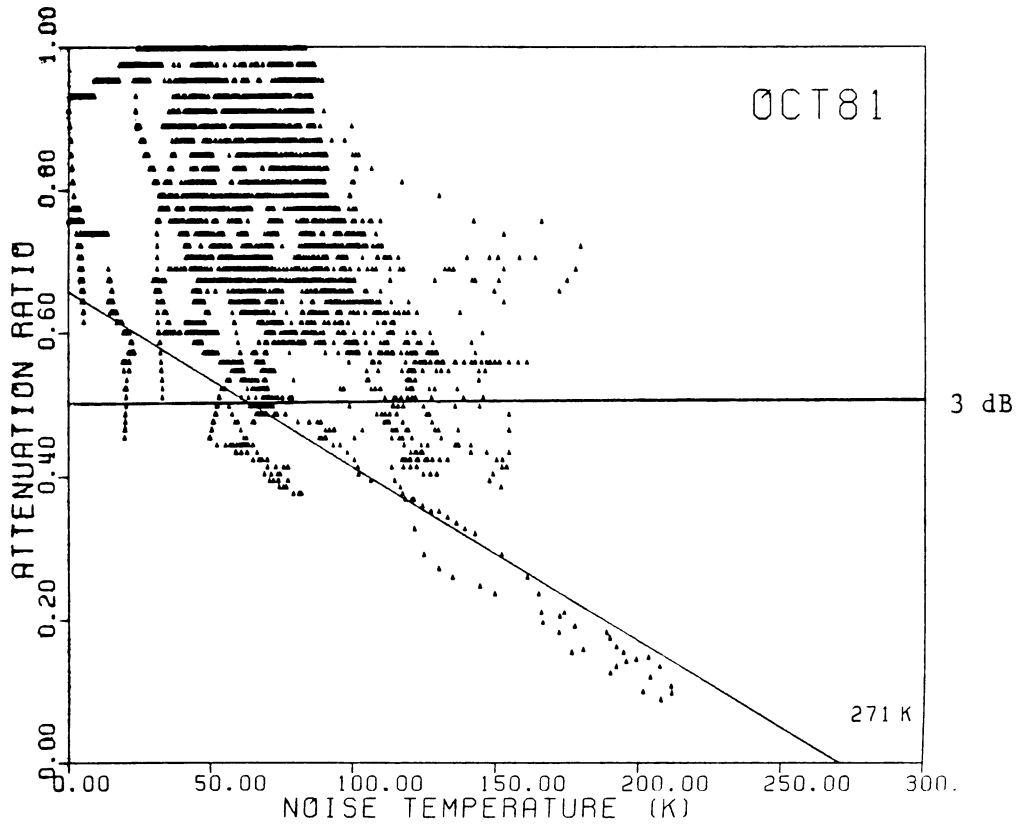


Figure 4.2-8 - Scatter Plot of Beacon Attenuation Ratio versus Sky Noise Temperature for October 1981, at 12 GHz, 10.7 degrees elevation angle, Blacksburg, VA (Linear regression applied only to points below line)

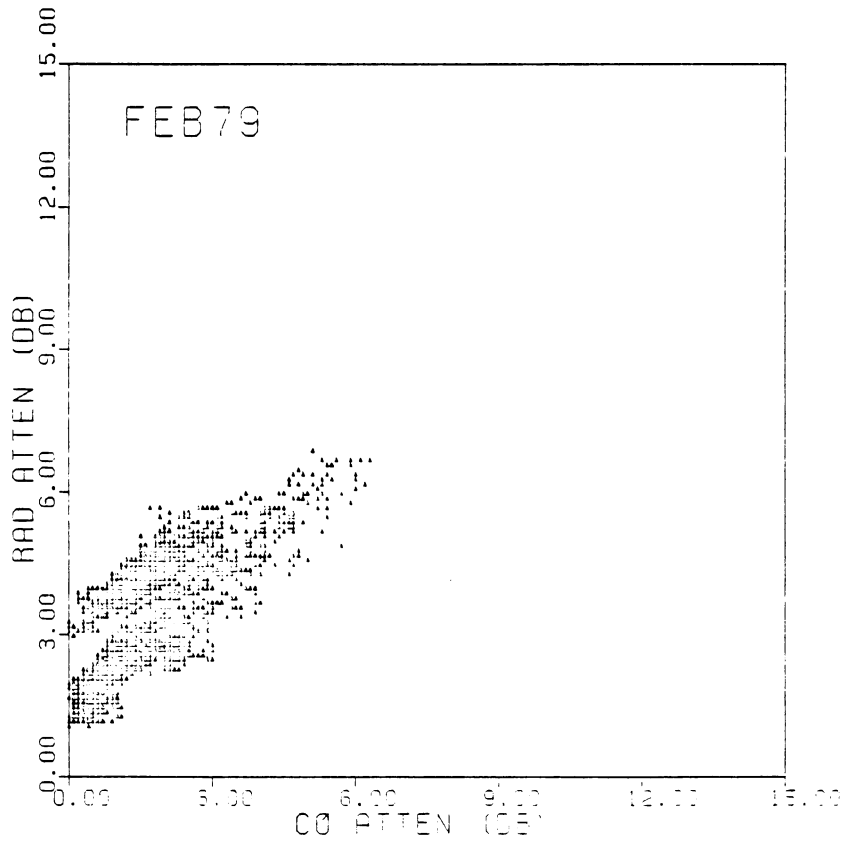


Figure 4.2-9 - Beacon Attenuation versus Radiometer Predicted Attenuation ($T_m = 265$ K) for February 1979, at 12 GHz, 10.7 degrees elevation angle, Blacksburg, VA

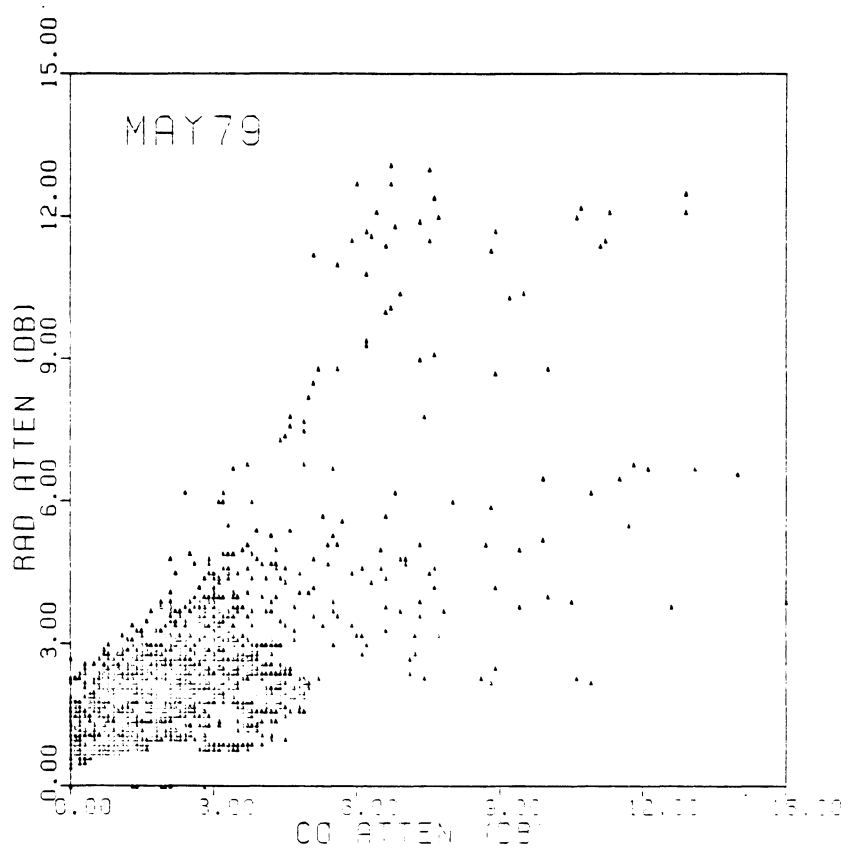


Figure 4.2-10 - Beacon Attenuation versus Radiometer Predicted Attenuation ($T_m = 265$ K) for May 1979, at 12 GHz, 10.7 degrees elevation angle, Blacksburg, VA

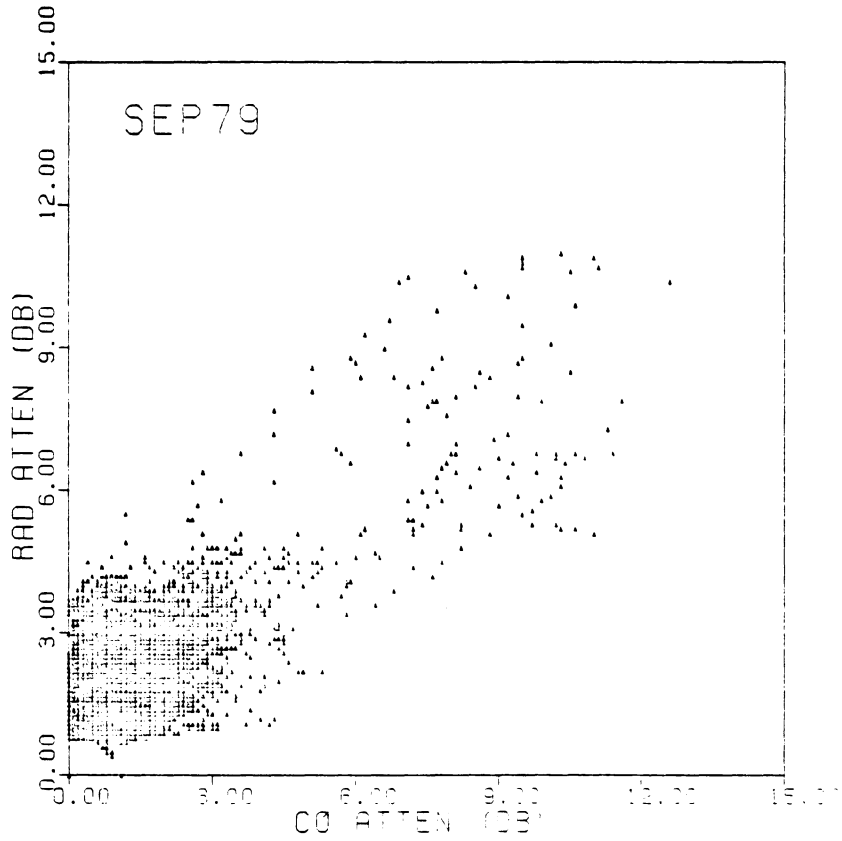


Figure 4.2-11 - Beacon Attenuation versus Radiometer Predicted Attenuation ($T_m = 265$ K) for September 1979, at 12 GHz, 10.7 degrees elevation angle, Blacksburg, VA

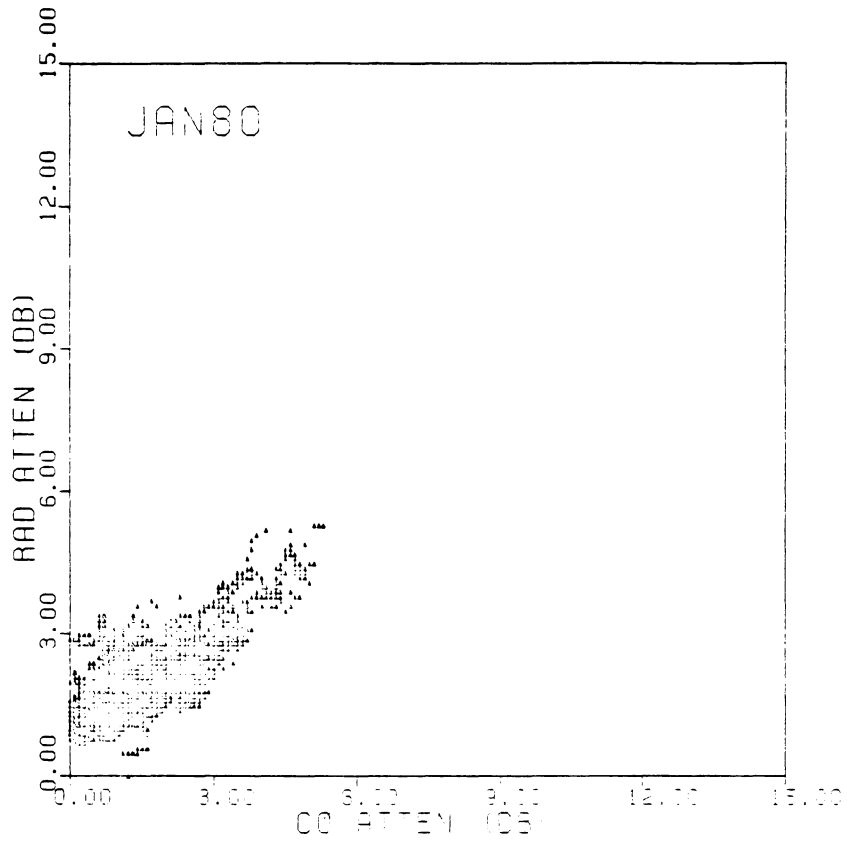


Figure 4.2-12 - Beacon Attenuation versus Radiometer Predicted Attenuation ($T_m = 265$ K) for January 1980, at 12 GHz, 10.7 degrees elevation angle, Blacksburg, VA

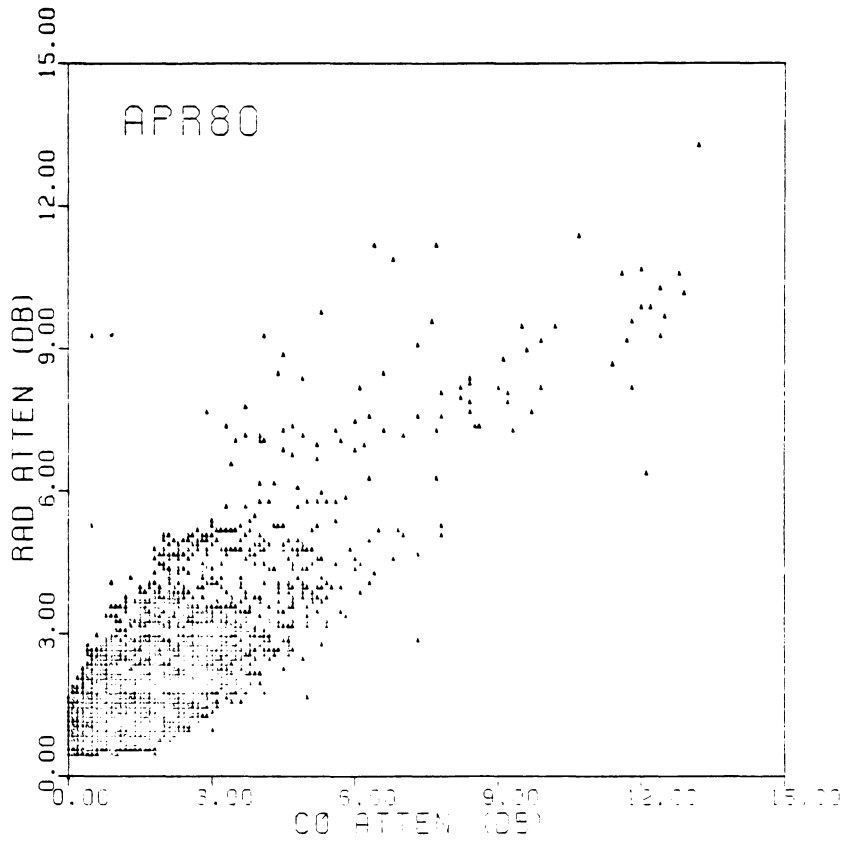


Figure 4.2-13 - Beacon Attenuation versus Radiometer Predicted Attenuation ($T_m = 265$ K) for April 1980, at 12 GHz, 10.7 degrees elevation angle, Blacksburg, VA

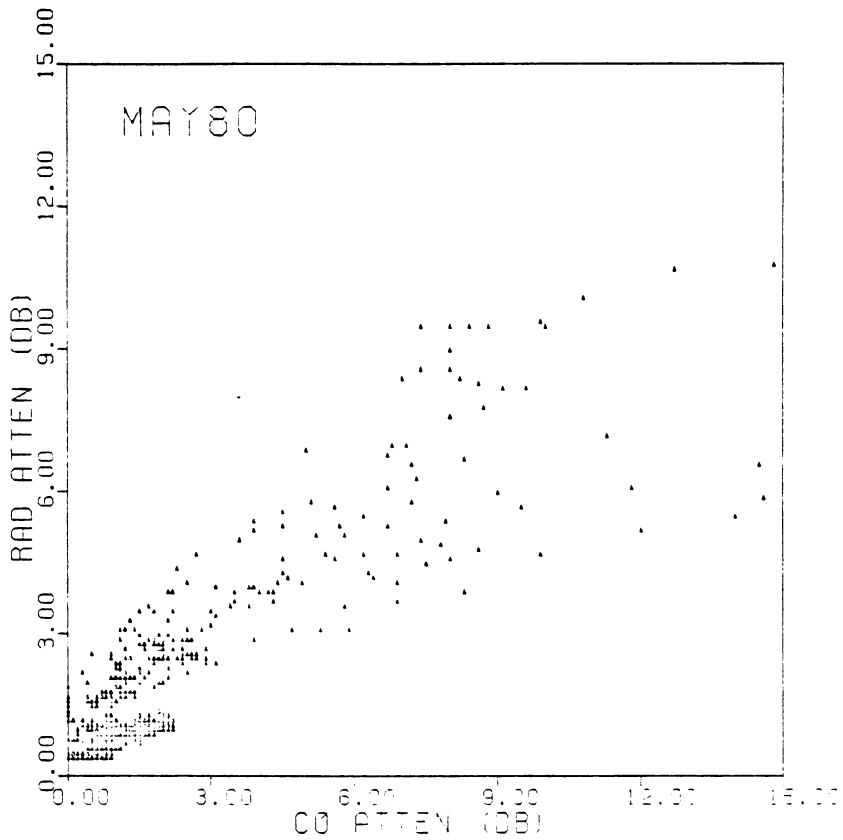


Figure 4.2-14 - Beacon Attenuation versus Radiometer Predicted Attenuation ($T_m = 265$ K) for May 1980, at 12 GHz, 10.7 degrees elevation angle, Blacksburg, VA

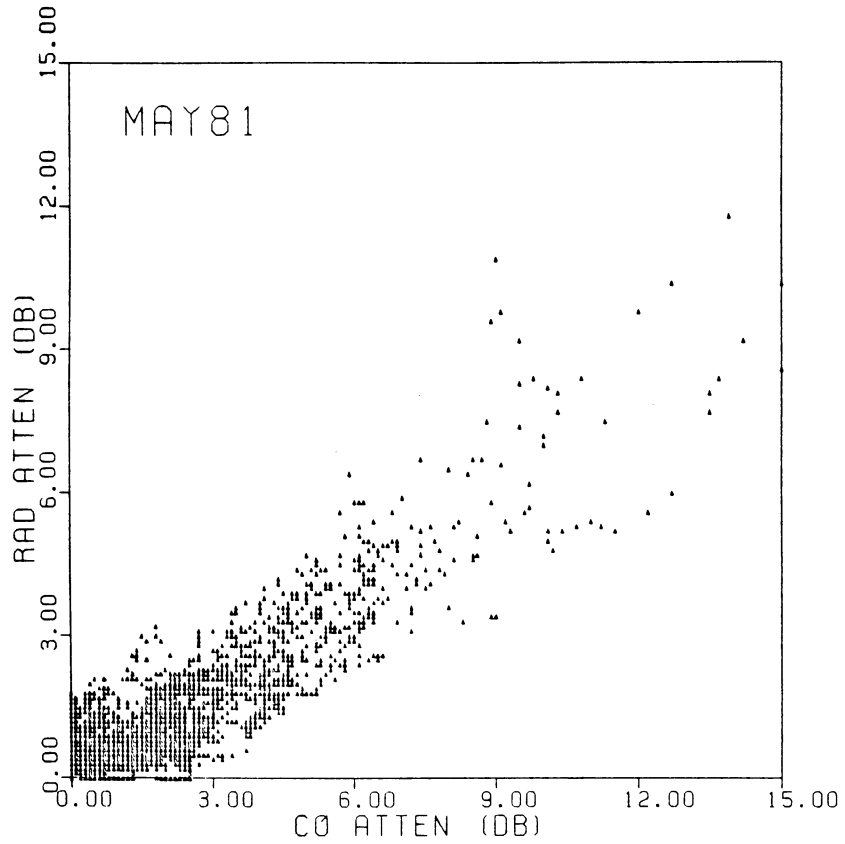


Figure 4.2-15 - Beacon Attenuation versus Radiometer
Predicted Attenuation ($T_m = 265$ K)
for May 1981, at 12 GHz, 10.7
degrees elevation angle, Blacksburg, VA

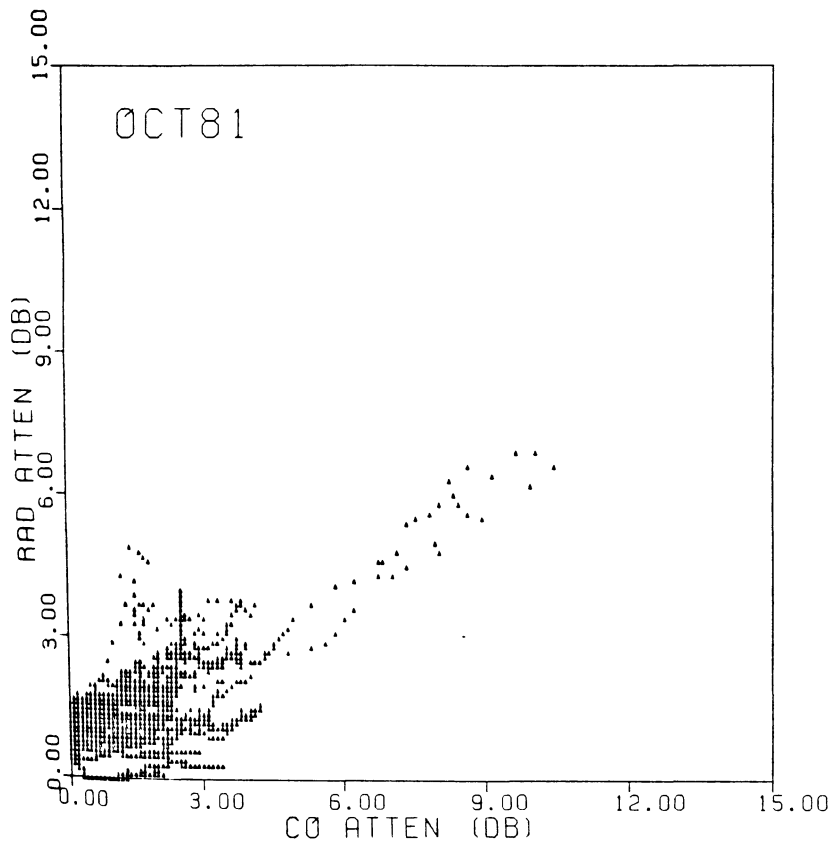


Figure 4.2-16 - Beacon Attenuation versus Radiometer Predicted Attenuation ($T_m = 265$ K) for October 1981, at 12 GHz, 10.7 degrees elevation angle, Blacksburg, VA

Chapter V
RADIOMETRIC EVENTS

5.1 DETERMINATION OF EVENTS

Events were determined by looking at the strip chart records for the entire three year period. A period of time was classified as an event if any one of the three following criteria were met:

1. Attenuation on the the copolar link exceeded 3 dB,
2. Isolation between the copolar and crosspolar channels dropped below 26 dB,
3. Attenuation predicted by the radiometer exceeded 3 dB.

This report does not use the isolation data and since these criteria are sometimes difficult to ascertain by the eye, some events contain no significant data. Many other events which meet the second condition show little or no attenuation (either copolar or radiometric). The events usually contain a period of clear air before and after the event for setting the attenuation reference levels. Table 5-1 presents the accumulated data for 1979 and includes the subset of significant radiometric events. Tables 5-2 and 5-3 show the events for 1980 and 1981, respectively. Some events contained large amounts of attenuation predicted from

the radiometer which were not included in the original statistical data base. It was clear that during these events the radiometer was malfunctioning and produced erroneous results. These events will be analyzed separately in Chapter VI.

The totals for the three years of data are 1671 hours of events and 780 hours of useful radiometer events. This amount of time includes many hours of signals that don't exceed the minimum thresholds. The radiometer attenuation exceeds 3 dB for 158.0 hours and the copolar attenuation exceeds 3 dB for 112.1 hours.

5.2 COMPARISON TO THE SATELLITE DOWNLINK

The radiometer operates without a satellite signal but the accuracy of the radiometer system can be checked by correlating radiometer predicted attenuation with the satellite copolar attenuation.

The satellite signal was provided by the Italian satellite, SIRIO, at 11.6 GHz. The radiometer, at 12 GHz with a 100 MHz bandwidth, was not affected by this signal. The satellite signal was received by a dual polarized 12 foot parabolic antenna with a final post-detection bandwidth of 0.1 Hz for best noise performance. The output voltage was converted to an arbitrary signal level in dBm. Then a

Table 5-1 - Distribution and Duration of Events for 1979

Month	Number of Events	Duration (hours)	Radiometer Events	Duration (hours)
January	11	32.063	1	7.515
February	3	19.634	3	19.643
March	11	36.822	3	19.220
April	8	21.346	3	12.757
May	13	19.826	6	13.736
June	25	45.824	11	25.551
July	31	125.992	11	58.355
August	20	80.455	11	54.667
September	20	73.324	6	37.840
October	12	50.699	1	11.180
November	16	82.167	0	0.0
December	5	45.466	0	0.0
Totals	175	633.618	56	260.474

Table 5-2 - Distribution and Duration of Events for 1980

Month	Number of Events	Duration (hours)	Radiometer Events	Duration (hours)
January	11	80.959	3	22.499
February	6	29.326	2	6.772
March	15	72.141	6	39.676
April	23	75.909	8	43.792
May	8	33.385	1	5.502
June	9	34.881	5	16.607
July	20	77.737	12	59.482
August	13	42.833	7	21.833
September	9	44.500	5	31.500
October	5	25.500	2	13.000
November	6	32.500	3	24.000
December	1	4.500	0	0.0
Totals	126	554.171	54	284.663

Table 5-3 - Distribution and Duration of Events for 1981

Month	Number of Events	Duration (hours)	Radiometer Events	Duration (hours)
January	0	0.0	0	0.0
February	7	27.888	2	13.217
March	2	19.817	1	9.682
April	9	23.399	4	12.649
May	14	59.689	6	35.078
June	13	31.895	7	22.906
July	23	95.571	10	50.818
August	9	40.156	3	21.670
September	12	57.950	6	41.380
October	10	88.060	3	27.808
November	2	5.766	0	0.0
December	8	32.519	0	0.0
Totals	109	482.710	42	235.208

zero reference level was set for each event to determine the excess attenuation. The radiometer system only gives reliable attenuation data up to 15 dB, so all values of attenuation beyond 15 dB on the copolar link are ignored in the analysis.

As seen in the scatter plots, Figures 4.2-9 through 4.2-16, the radiometer often shows good agreement within ± 1 dB uncertainty bounds. However, some of the months, May 1979 in particular, seem to miss the center line (perfect correlation). They exhibit a wide spread of points on either side of the center line. This indicates that both the radiometer and the beacon signal observed a similar attenuation level but not at the same time. High attenuation levels don't last very long and it is possible for the two signals to become de-correlated by small timing errors between the two signals.

In Figures 5.2-1 through 5.2-4 are plotted four events. These are typical events with large attenuation levels. The scatter plots of the beacon attenuation ratio versus the sky noise temperature are shown in Figures 5.2-5 to 5.2-8. All analysis is performed only on points between 3 and 15 dB. The event on 25 February 1979 extends only up to 7 dB of attenuation but shows very strong correlation. The 19 August 1979 event shows a broad scattering of points at

lower attenuation but as the attenuation rises, the correlation between the two signals becomes much better. An event such as the one on 8 July 1980 is not well correlated. There are points of large radiometric attenuation and small beacon attenuation and vice-versa. The medium temperatures predicted by these events fluctuate wildly, from a low of 202 K to a high of 279 K. Some events predict medium temperatures of over 300 K. This is the reason only long-term statistics compiled by a radiometer have any real meaning.

One type of long term statistic is exceedence. Exceedence is defined as the percent of time that a signal exceeds a given level, in this case, attenuation. Three exceedence plots are shown in Figures 5.2-9, 5.2-10, and 5.2-11. The BEACON is the copolar attenuation, the BEACON W/OFFSET includes the 0.4 dB offset level, and RADIOMETER is the radiometer predicted attenuation. The plots extend from 3 dB to 15 dB of attenuation. The first plot, for 1979, shows excellent agreement with the beacon attenuation. It overpredicts slightly at the low attenuation values and slightly at the highest values. Around 14 or 15 dB the radiometer becomes very sensitive to small changes in sky noise temperature and the curve will flatten out if continued to 20 dB. The 1980 data slightly underpredicts the

attenuation up to 8 dB. Past the 8 dB point there is about a 2 dB gap between the curves. More than two-thirds of the data points at these attenuation levels occurred in July 1980 and the radiometer seems to have consistently underestimated the data by 1-2 dB during this month. The 1981 exceedence plot also predicts attenuation 1 to 2 dB less than the beacon attenuation. The radiometer does not record as much attenuation during sharp attenuation spikes (heavy rain) as seen by the satellite signal.

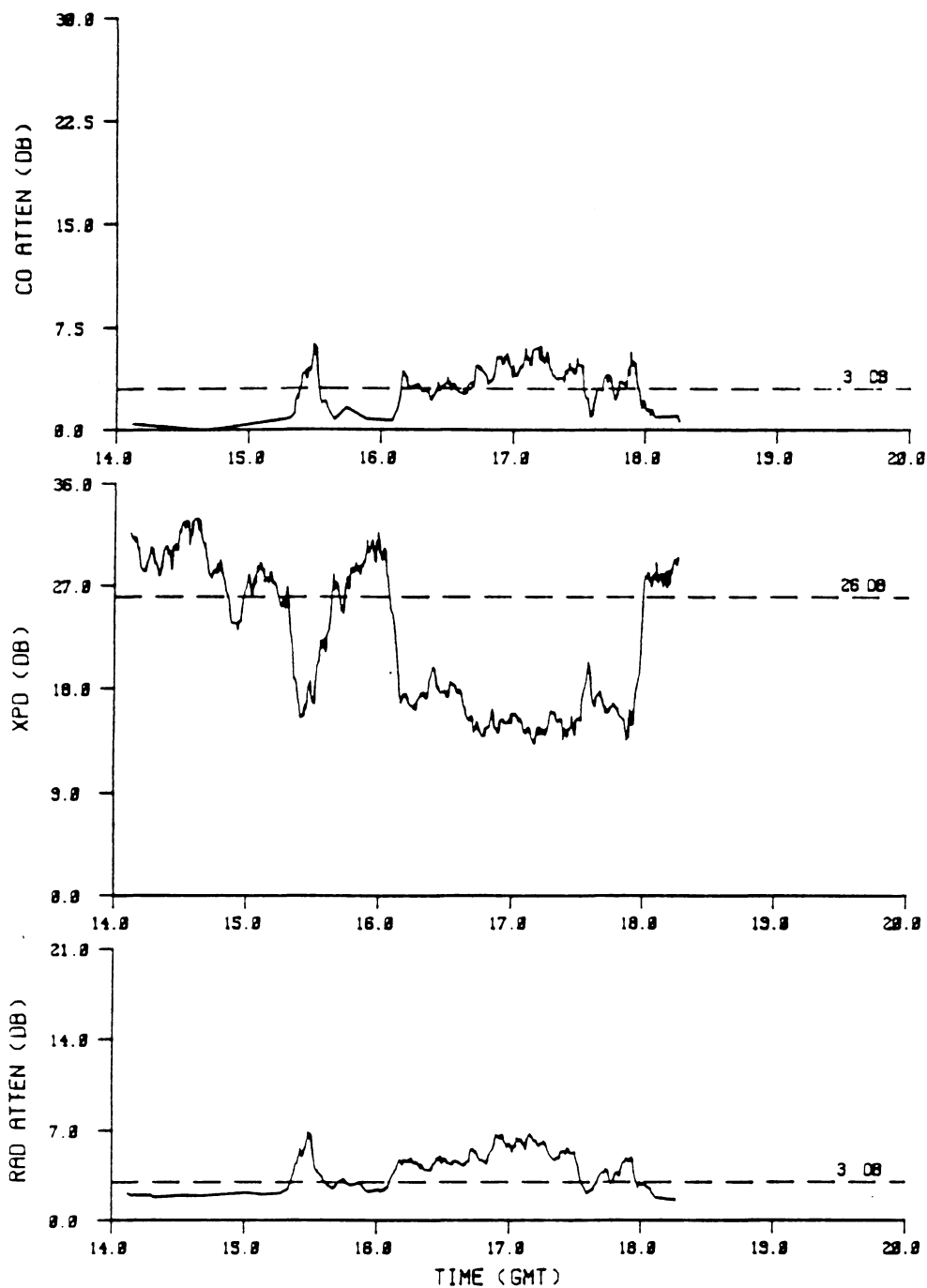


Figure 5.2-1 - Plot of Event on 25 February 1979,
 at 12 GHz, 10.7 degrees elevation angle.
 Beacon attenuation is the top plot and
 radiometer predicted attenuation is the
 bottom plot.

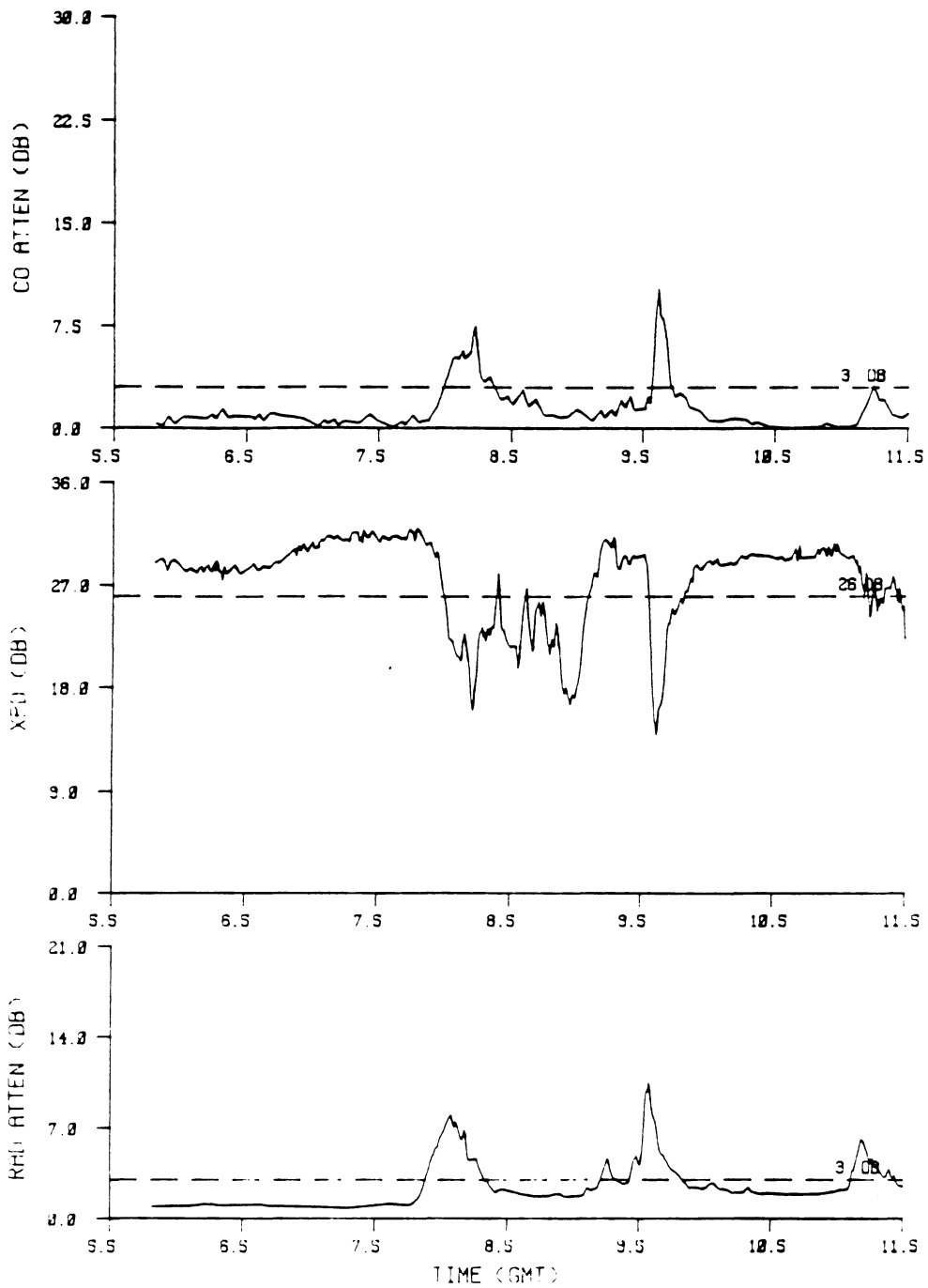


Figure 5.2-2 - Plot of Event on 19 August 1979,
 at 12 GHz, 10.7 degrees elevation angle.
 Beacon attenuation is the top plot and
 radiometer predicted attenuation is the
 bottom plot.

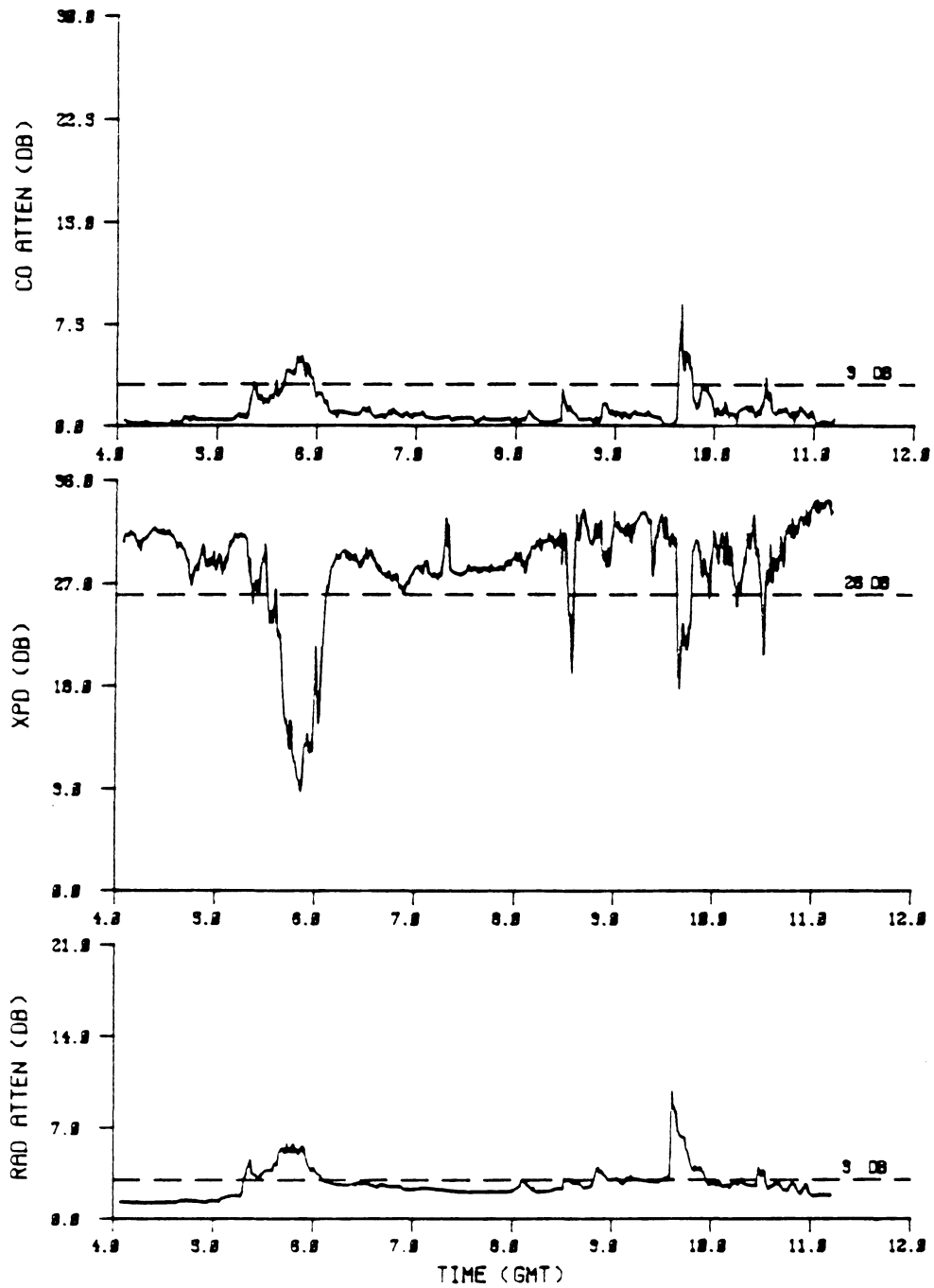


Figure 5.2-3 - Plot of Event on 4 April 1980, at 12 GHz, 10.7 degrees elevation angle. Beacon attenuation is the top plot and radiometer predicted attenuation is the bottom plot.

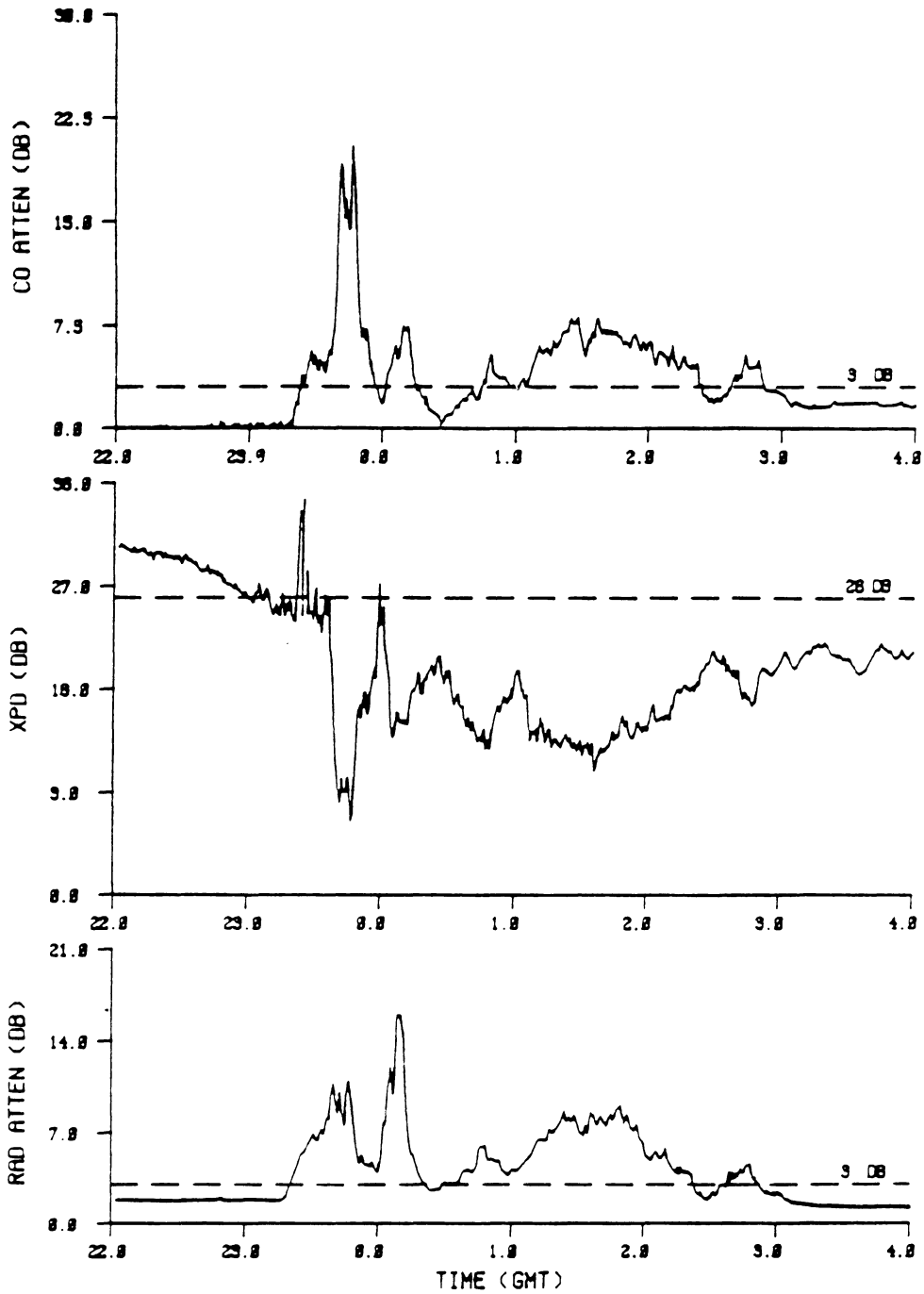


Figure 5.2-4 - Plot of Event on 8 July 1980, at 12 GHz, 10.7 degrees elevation angle. Beacon attenuation is the top plot and radiometer predicted attenuation is the bottom plot.

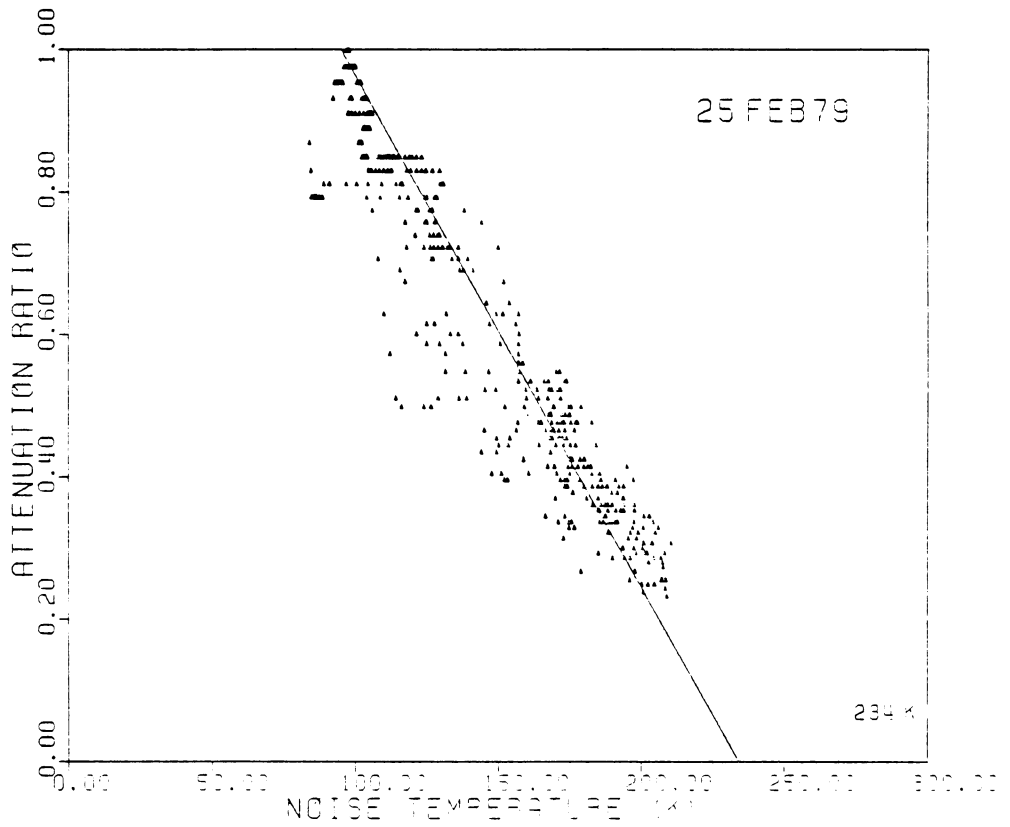


Figure 5.2-5 - Scatter Plot of Beacon Attenuation Ratio versus Sky Noise Temperature for Event on 25 February 1979, at 12 GHz, 10.7 degrees elevation angle, Blacksburg, VA

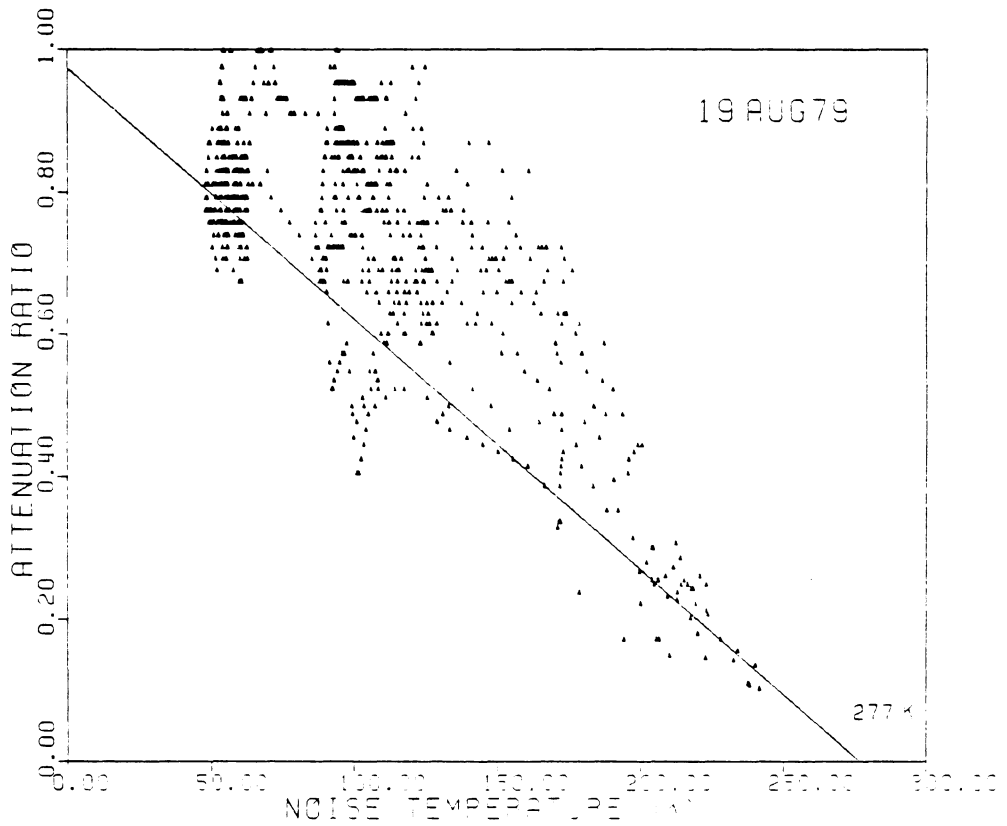


Figure 5.2-6 - Scatter Plot of Beacon Attenuation Ratio versus Sky Noise Temperature for Event on 19 August 1979, at 12 GHz, 10.7 degrees elevation angle, Blacksburg, VA.

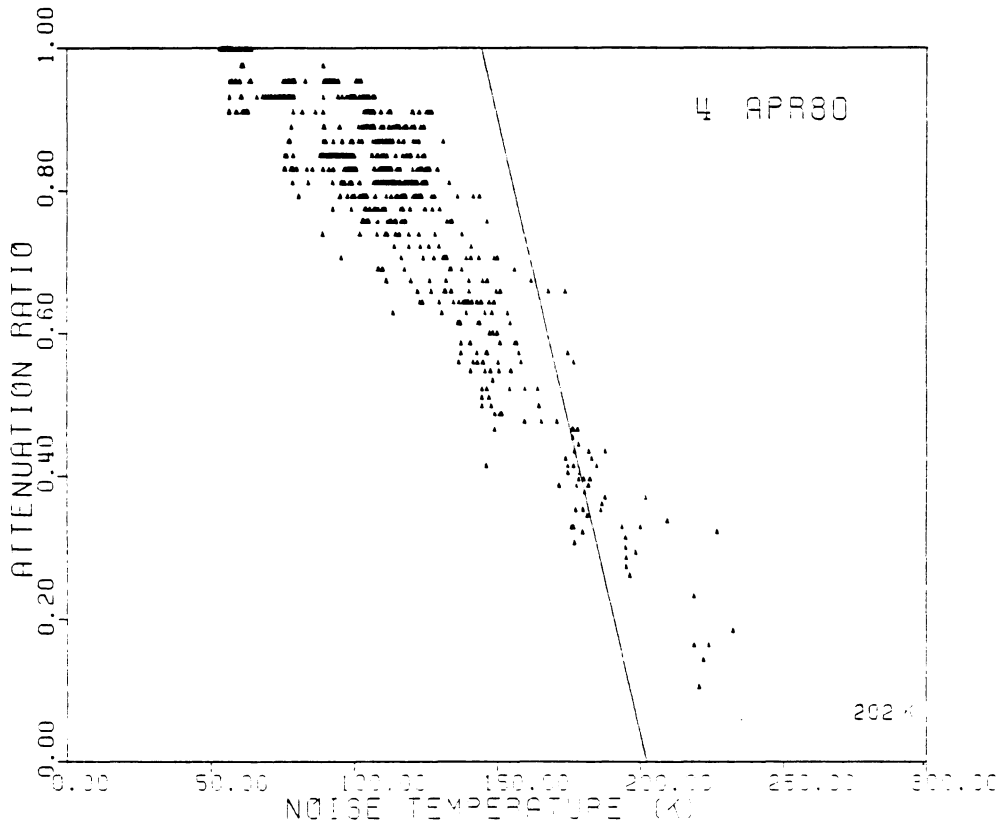


Figure 5.2-7 - Scatter Plot of Beacon Attenuation Ratio versus Sky Noise Temperature for Event on 4 April 1980, at 12 GHz, 10.7 degrees elevation angle, Blacksburg, VA.

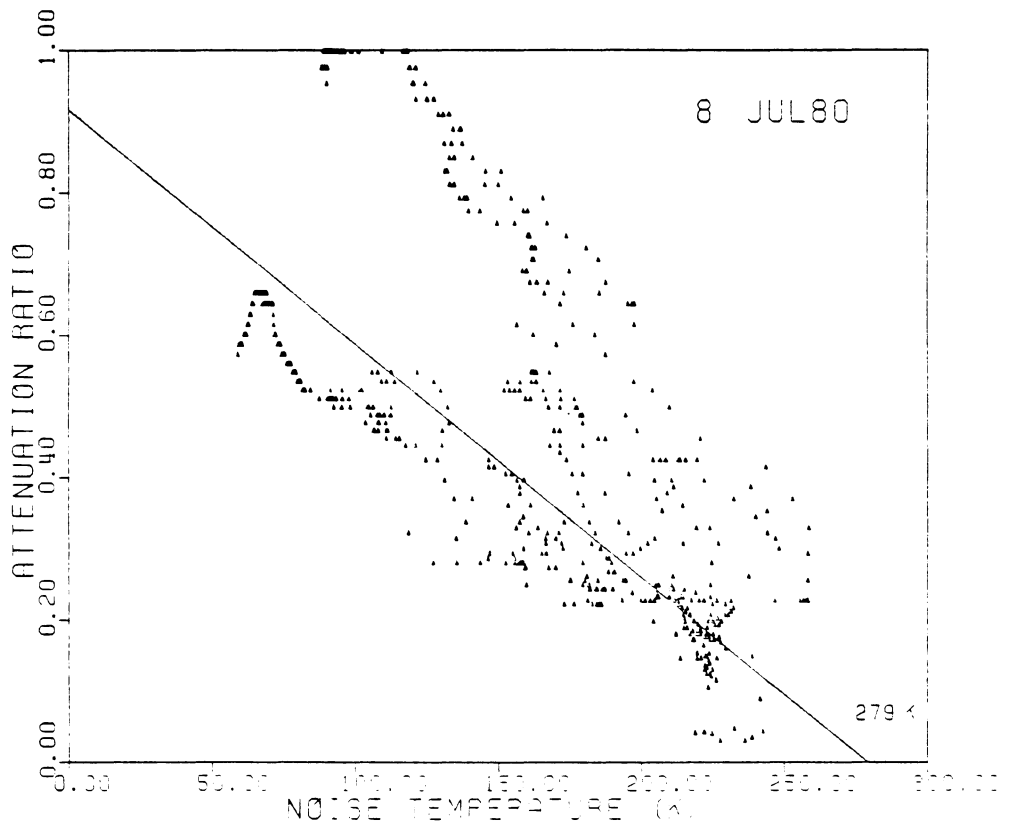


Figure 5.2-8 - Scatter Plot of Beacon Attenuation Ratio versus Sky Noise Temperature for Event on 8 July 1980, at 12 GHz, 10.7 degrees elevation angle, Blacksburg, VA.

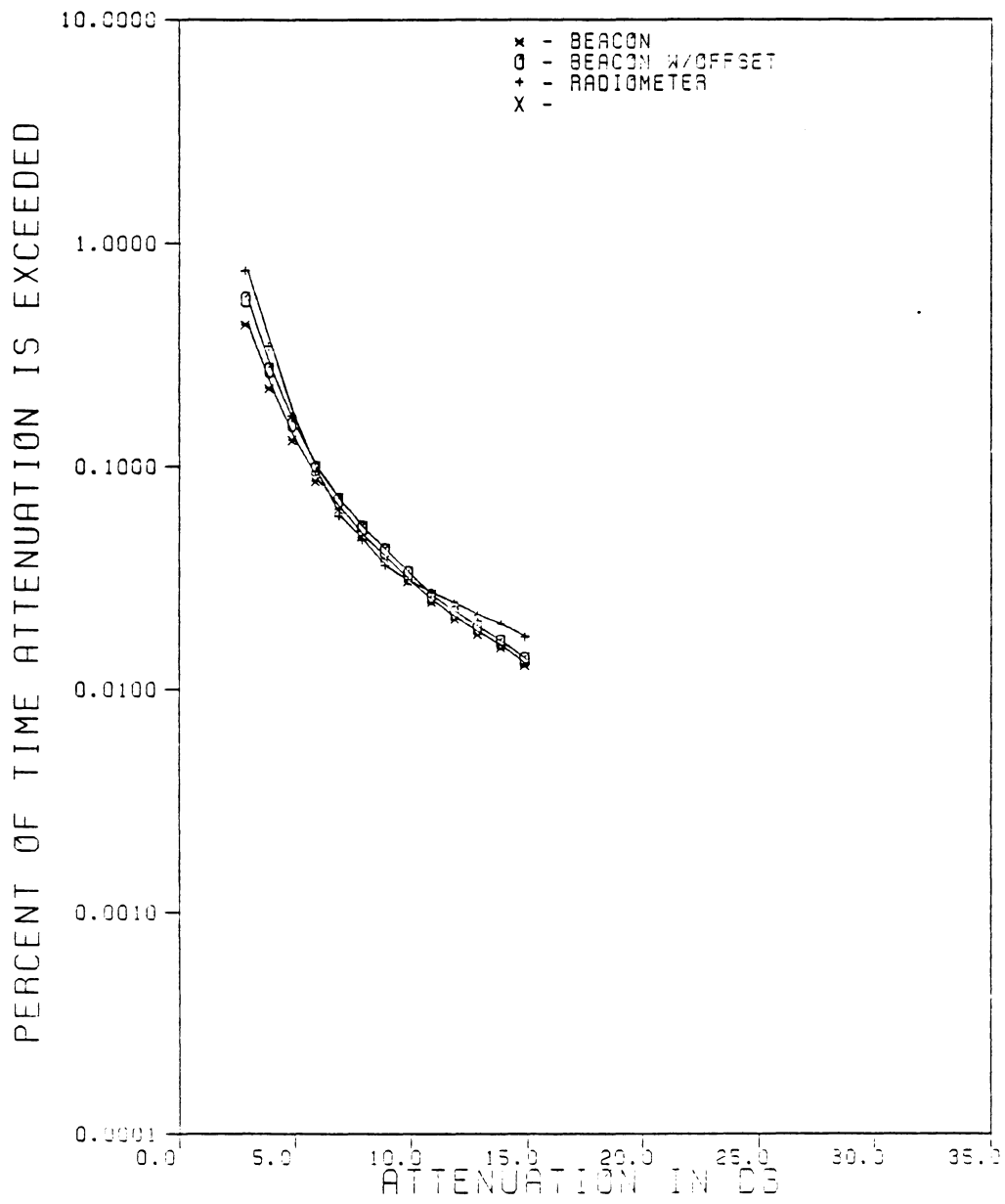


Figure 5.2-9 - Exceedence Plot for 1979 Data Set

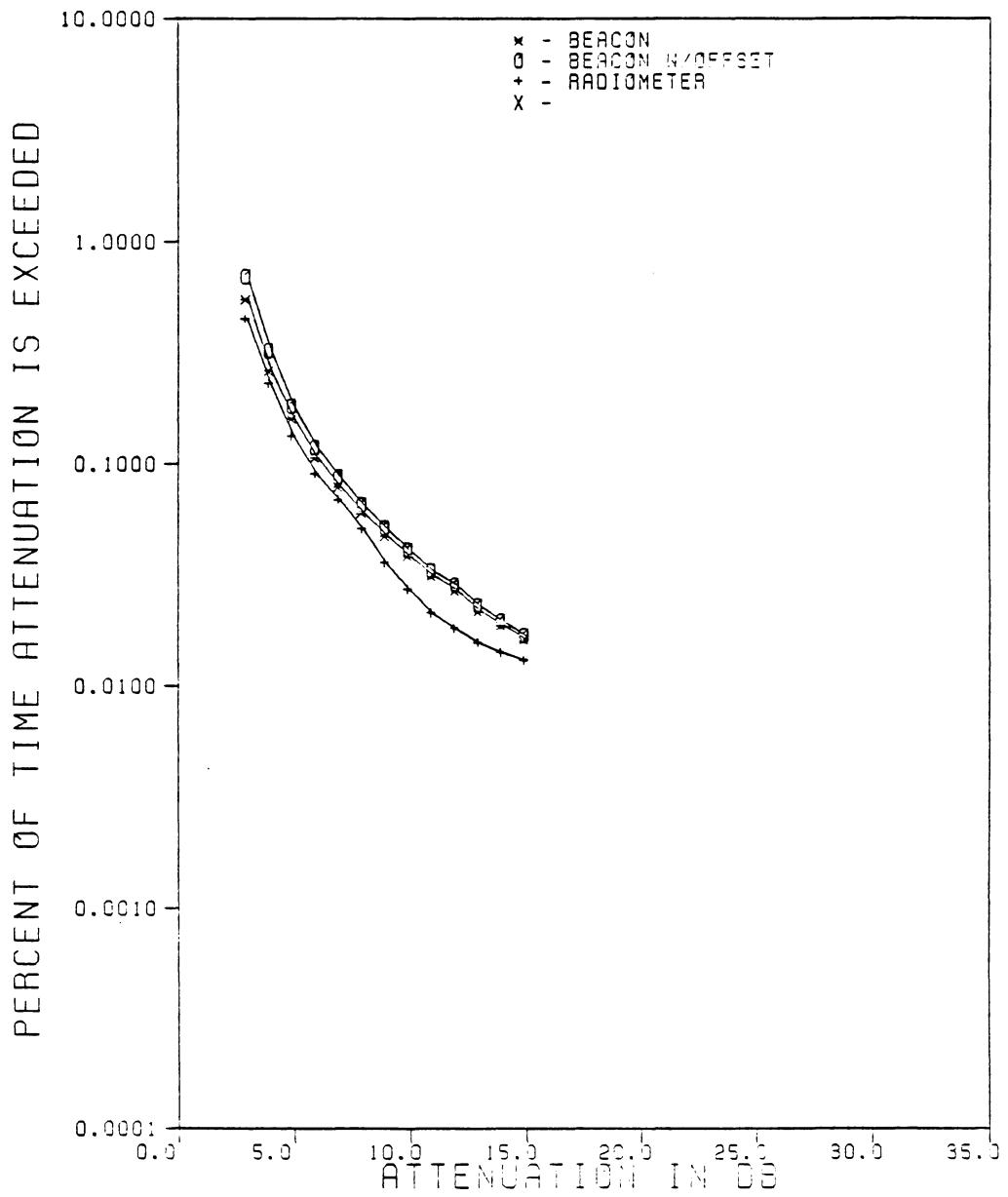


Figure 5.2-10 - Exceedence Plot for 1980 Data Set

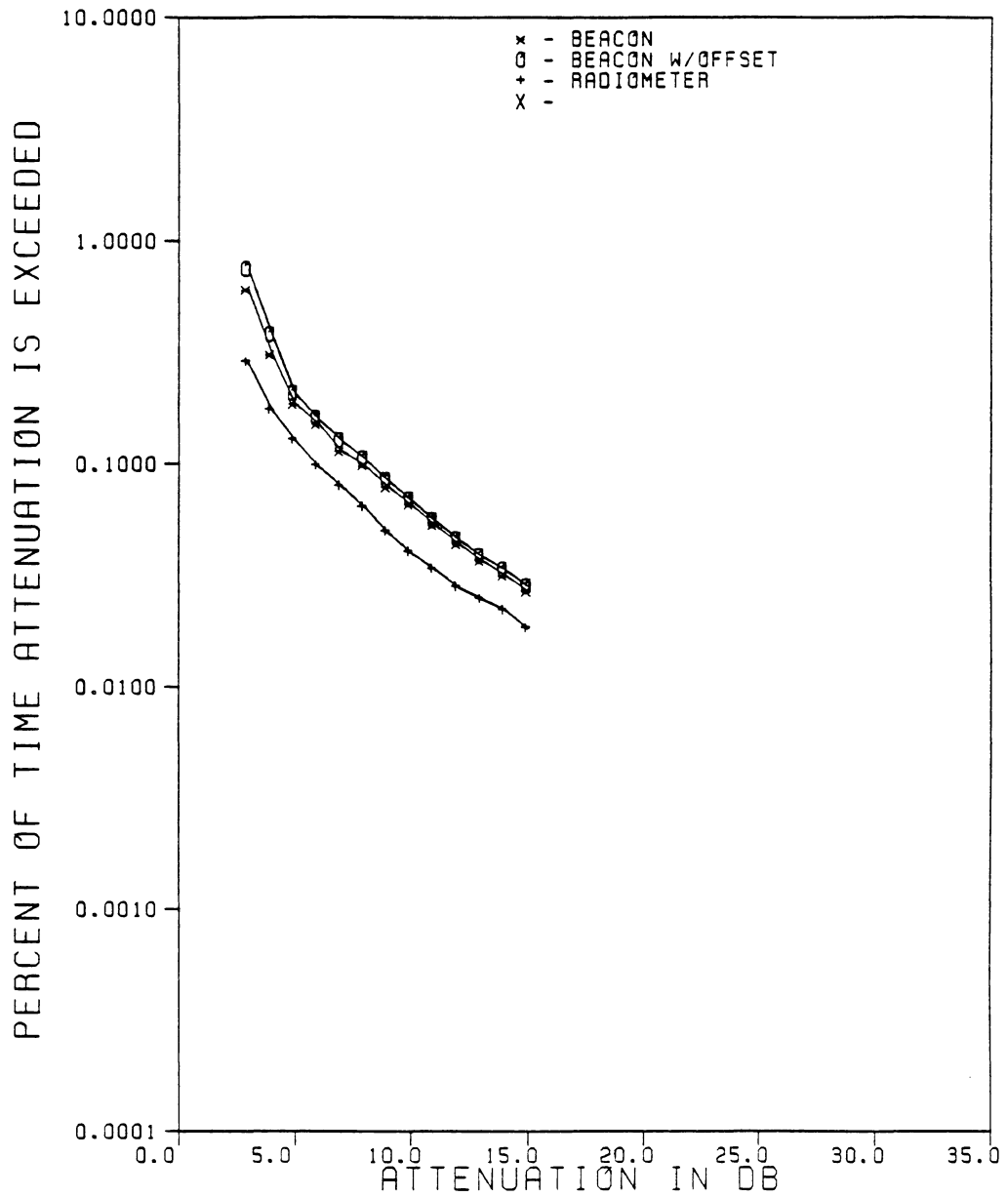


Figure 5.2-11 - Exceedence Plot for 1981 Data Set

Chapter VI

RADIOMETER PERFORMANCE DURING THE SIRIO EXPERIMENT

6.1 DISCUSSION OF THE OPERATION OF THE RADIOMETER

Over the entire three year duration of the SIRIO experiment the radiometer was operated unattended, except during manual calibrations. During the analysis of the data some sky noise temperatures recorded by the radiometer were noticed to be very suspect. The baseline, which should be around 20 to 50 K in clear weather, drifted up to 150 K for long periods of time. Some events (as determined by the copolar attenuation) occurred during these times and consequently gave radiometer predicted attenuation values of 3 dB or greater. Even in the presence of clouds (which frequently are present at the start or end of an event) the sky noise temperature should not exceed 80 K. In a few cases, the sky noise temperature started out at 200 K. The additional noise temperature must have been generated in the radiometer due to a fault mechanism outside the radiometer switching loop.

6.2 MODELING OF THE RADIOMETER

There could have been many reasons for the radiometer to malfunction and only one clue is available for suggesting a mechanism. As mentioned in section 3.5 the noise diode indicated changes in the gain outside of the Dicke-switching loop. Referring back to Figure 3.1-1 the most likely candidate for problems is the ferrite switch in the RF front end section. This is the only active device in the RF section which is not included in the loop. The model proposed in Figure 6.2-1 assumes an attenuation in the ferrite switch and is a best estimate of what might have gone astray. In the normal 'on' state the switch would typically have a loss of 0.2 dB. The 'off' state would give an attenuation (actually isolation between the two ports of the ferrite switch) of 30 dB. However, if the ferrite switch did not turn 'on' completely the attenuation could increase dramatically. If a lossy device is inserted between the antenna and the radiometer input port the apparent noise temperature, T_{in} , at the input of the radiometer IF section is

$$T_{in} = T_A L_A + T_P(1 - L_A) \quad (6.2.1)$$

with the additive noise diode turned off, and

$$T_{in} = (T_A + T_D)L_A + T_P(1 - L_A) \quad (6.2.2)$$

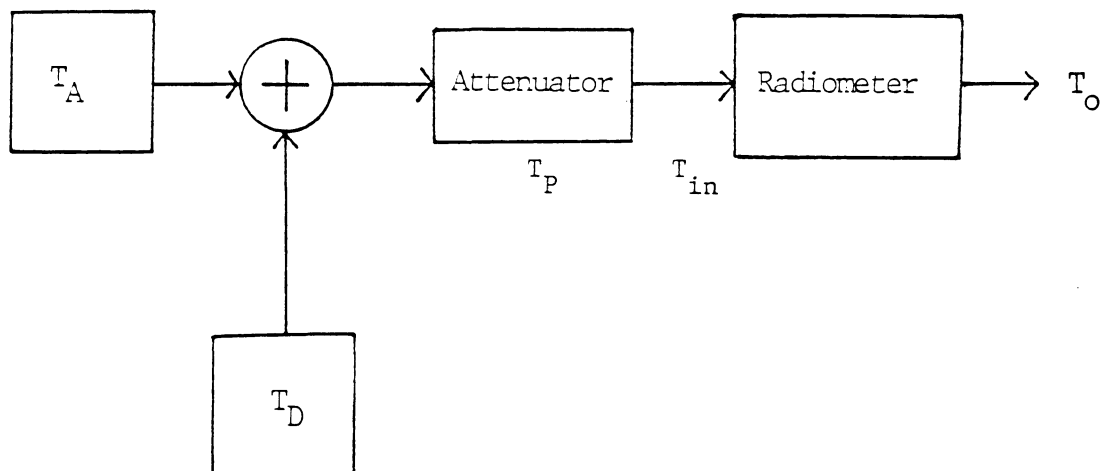


Figure 6.2-1 - Proposed Model of Radiometer Fault

with the inclusion of the noise diode temperature. In the equations above,

T_A = antenna and sky noise temperature

T_D = noise diode temperature

T_P = physical temperature of attenuating device

L_A = loss due to attenuation (expressed as a ratio)

The loss in decibels can be converted to a ratio for use in equations (6.2.1) and (6.2.2) by

$$L = 10^{(-\text{loss}/10)} \quad (6.2.3)$$

During manual calibrations the radiometer was assumed to be working correctly and the height (in inches) of the additive noise diode temperature can be used as the benchmark (i.e. $L = 0$ dB). With no loss, L_A is 1 and the two equations are

$$T_{\text{in}} = T_A \quad (6.2.4)$$

$$T_{\text{in}} = T_A + T_D \quad (6.2.5)$$

At the output of the radiometer the antenna temperature is subtracted out (by achieving a balanced condition) leaving only the output temperature, T_o . Substituting yields

$$T_{\text{app}} = T_o L_A + T_P(1 - L_A) \quad (6.2.6)$$

$$T_{\text{app}} = (T_o + T_D)L_A + T_P(1 - L_A) \quad (6.2.7)$$

where T_{app} = apparent output temperature with
attenuating device

T_o = output temperature without attenuating
device

T_{sky} can then be found from

$$T_{\text{sky}} = 1.04T_o - 16.46 \quad (3.4.6)$$

Subtracting equation (6.2.7) from (6.2.6) yields

$$T_{\text{diff}} = T_D L_A \quad (6.2.8)$$

or

$$L_A = T_{\text{diff}}/T_D \quad (6.2.9)$$

where T_{diff} = temperature difference between noise diode on
and off conditions

T_{diff} is simply the additive noise temperature of the noise diode during a suspect event. Since the noise temperature is linearly related to inches of deflection on the chart

$$L_A = \text{ND}_{\text{event}}/\text{ND}_{\text{manual}} \quad (6.2.9)$$

where ND_{event} = average additive (or delta) noise diode
height during the event

$\text{ND}_{\text{manual}}$ = delta noise diode height recorded during a
manual calibration

The physical temperature of the ferrite switch (attenuation device), T_p , is assumed to be 300 K. Equation (6.2.6) becomes

$$T_o = (T_{\text{app}} - 300(1 - L_A))/L_A \quad (6.2.10)$$

6.3 CORRECTION APPLIED TO THE EVENTS

Out of 175 recorded events in 1979, 27 were determined to contain bad radiometer data. Nineteen events out of 126 in 1980 were declared invalid and no events in 1981 exhibited this problem. These events were not included in the monthly or yearly statistics. By applying the corrective model proposed in the previous section these events could be used in the statistics.

All these events predict attenuation far in excess of the beacon attenuation. In Figures 6.3-1 to 6.3-6 the radiometer predicted attenuation is the top line (dashed) and the copolar attenuation is the bottom line. As can be seen the model does reduce the radiometer attenuation considerably. The reduction is not perfect with somewhat high levels still predicted when the beacon attenuation is nearly zero but the correction factor does show excellent correlation at the high levels of attenuation. The attenuation spikes in the events on 10 November 1979 (Figure 6.3-3), 24 December 1979 (Figure 6.3-5), and 24 March 1980 (Figure 6.3-6) are almost identical for both the radiometer and the beacon. Only some of the extra attenuation at low values can be attributed to the offset level (not included in these plots).

This model seems to provide a reasonable solution to the problems found in these events.

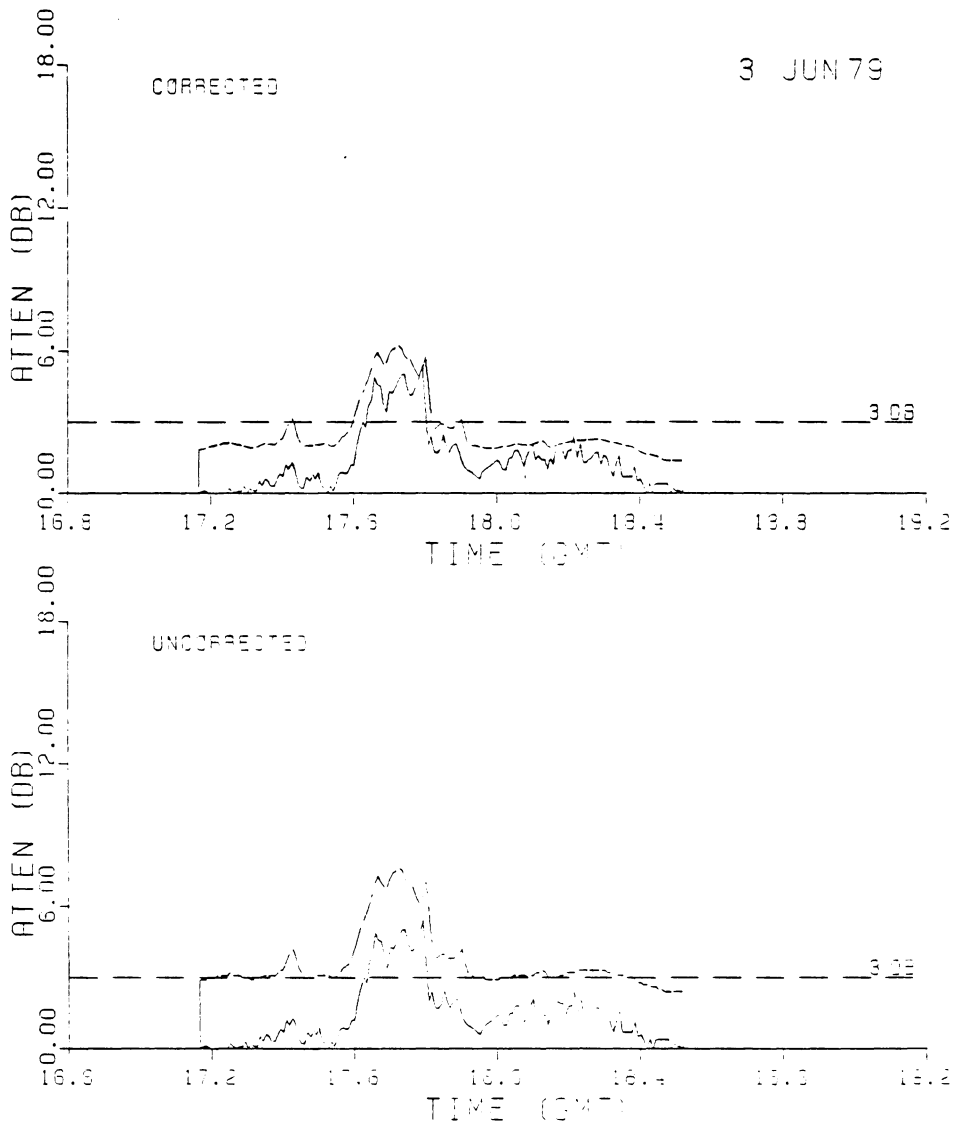


Figure 6.3-1 - Plot of Event on 3 June 1979.
Bottom plot shows invalid radiometer
attenuation (top line). Top plot shows
corrected radiometer data again plotted
with beacon attenuation.

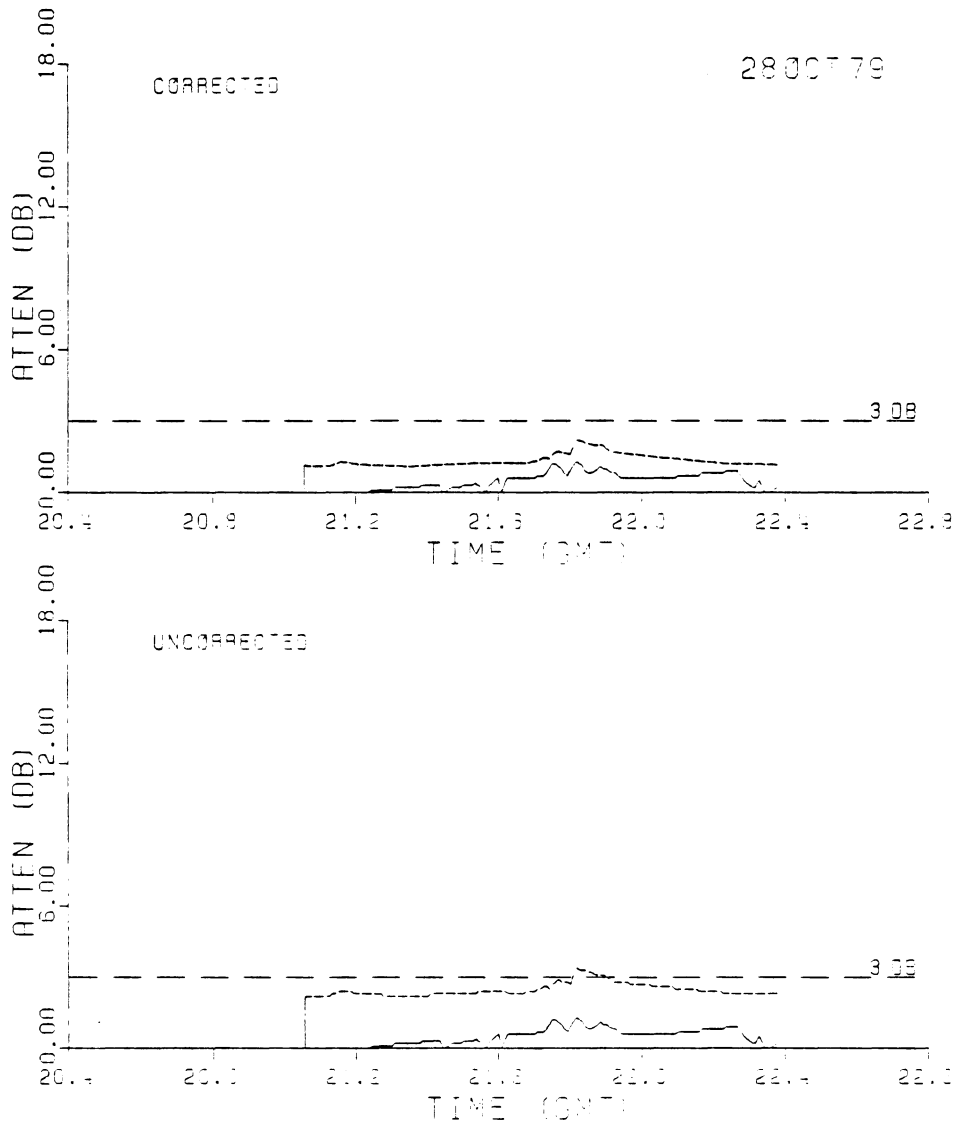


Figure 6.3-2 - Plot of Event on 28 October 1979. Bottom plot shows invalid radiometer attenuation (top line). Top plot shows corrected radiometer data again plotted with beacon attenuation.

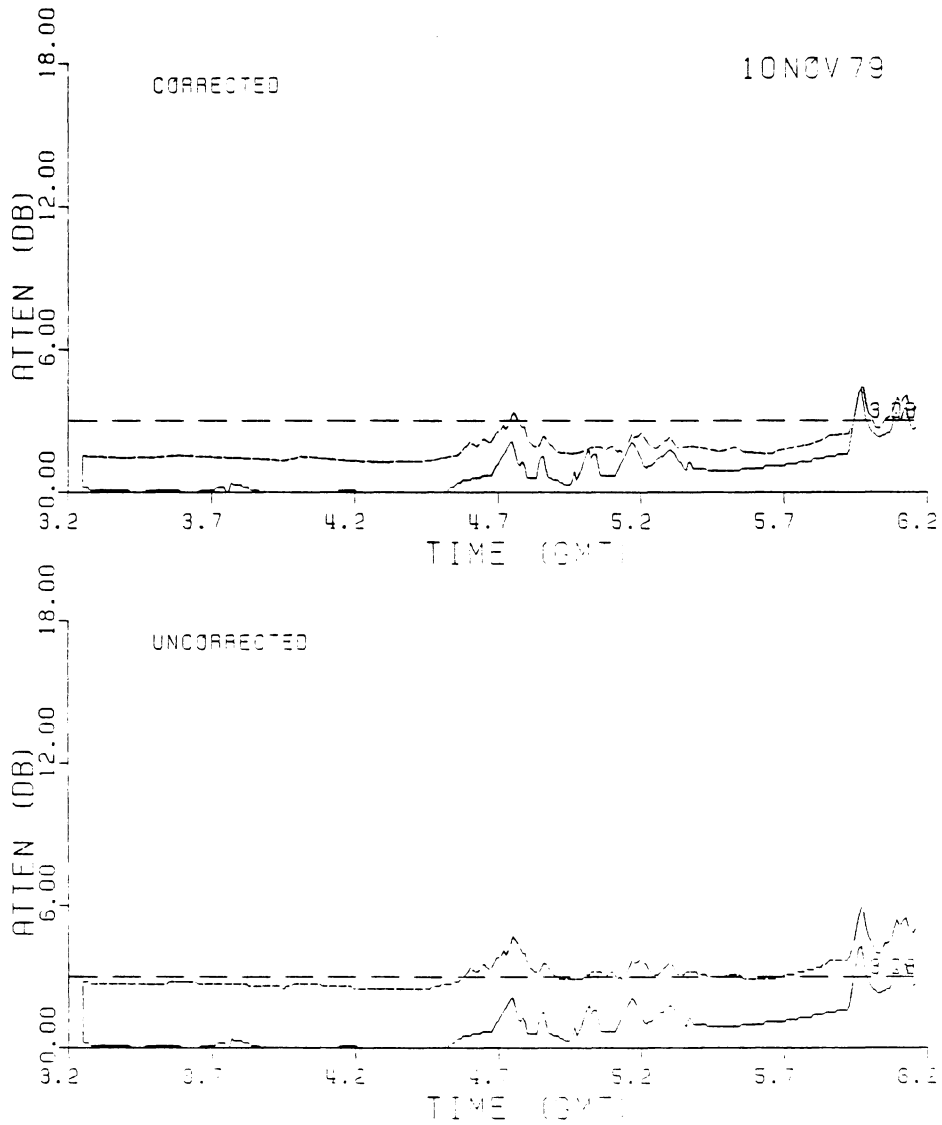


Figure 6.3-3 - Plot of Event on 10 November 1979. Bottom plot shows invalid radiometer attenuation (top line). Top plot shows corrected radiometer data again plotted with beacon attenuation.

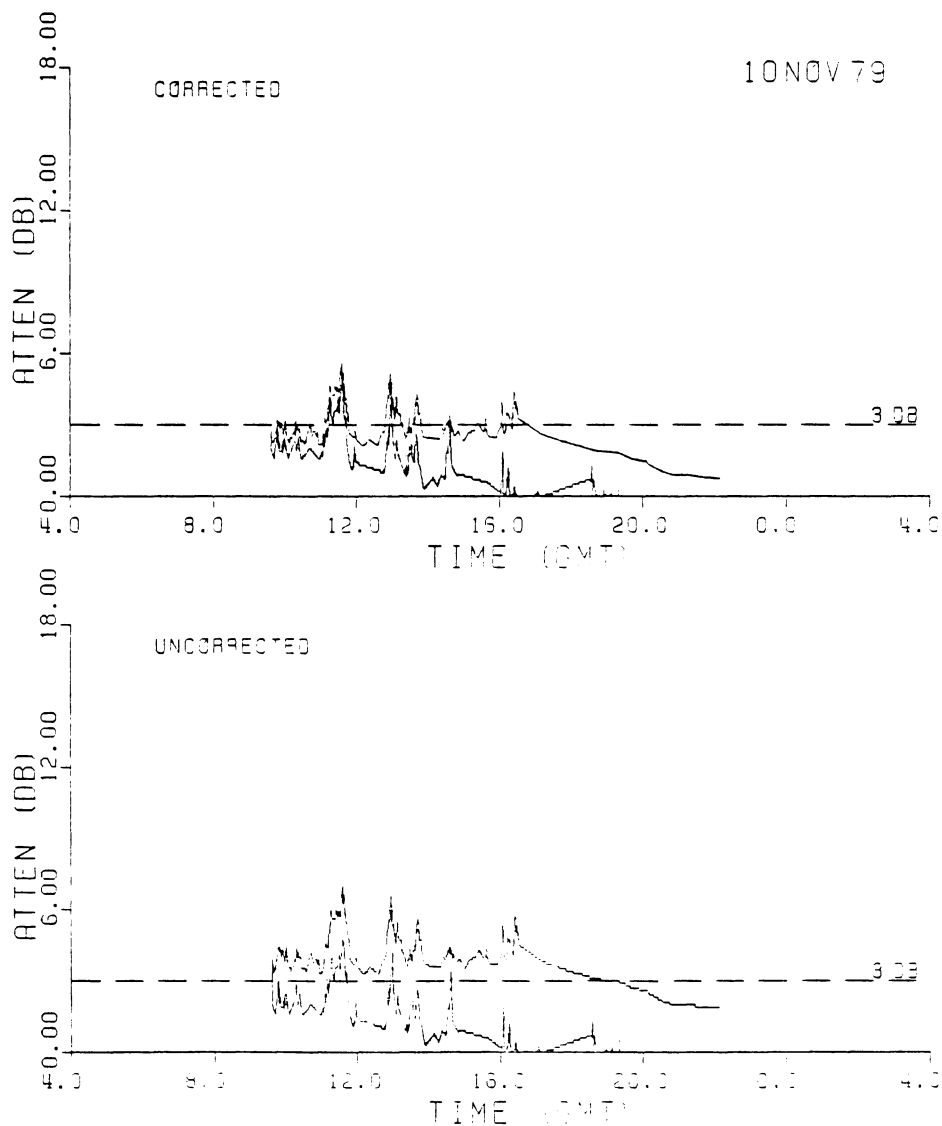


Figure 6.3-4 - Plot of Event on 10 November 1979. Bottom plot shows invalid radiometer attenuation (top line). Top plot shows corrected radiometer data again plotted with beacon attenuation.

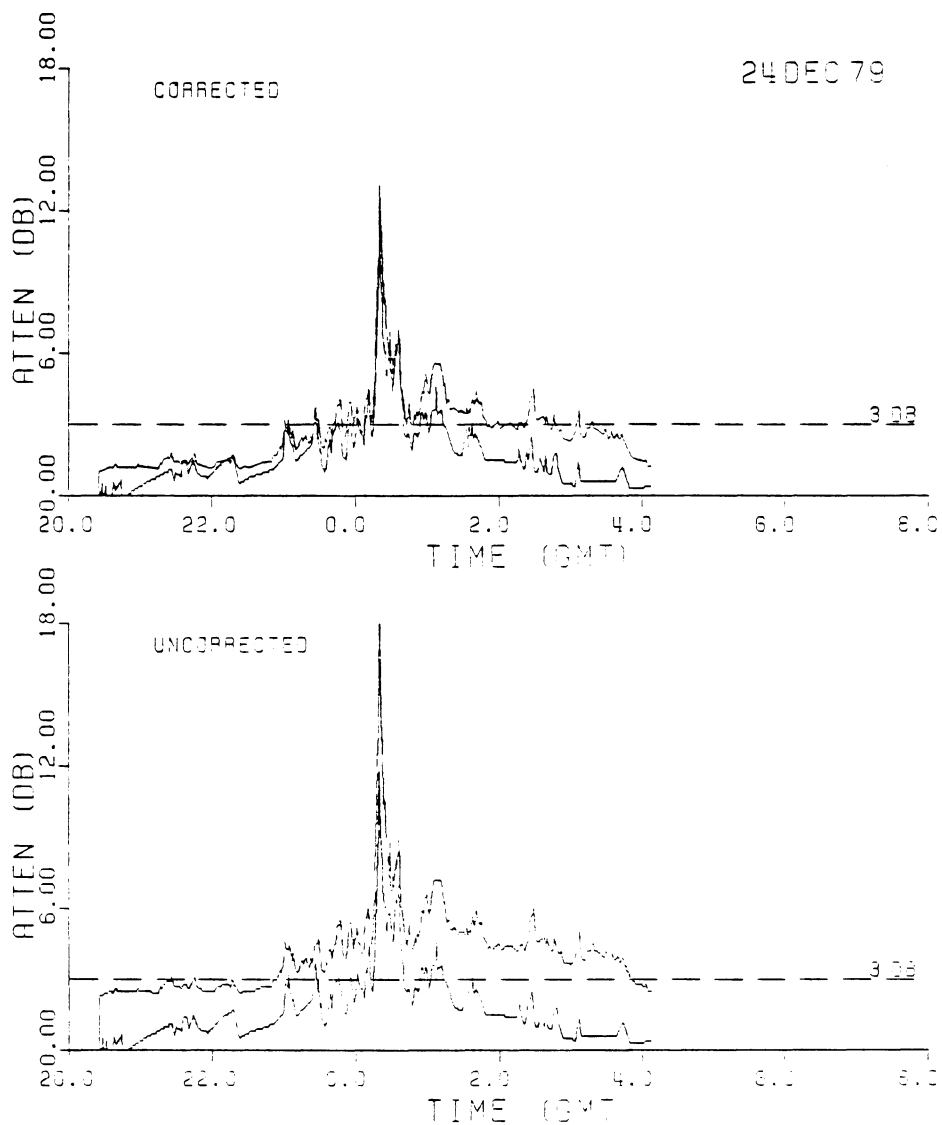


Figure 6.3-5 - Plot of Event on 24 December 1979. Bottom plot shows invalid radiometer attenuation (top line). Top plot shows corrected radiometer data again plotted with beacon attenuation.

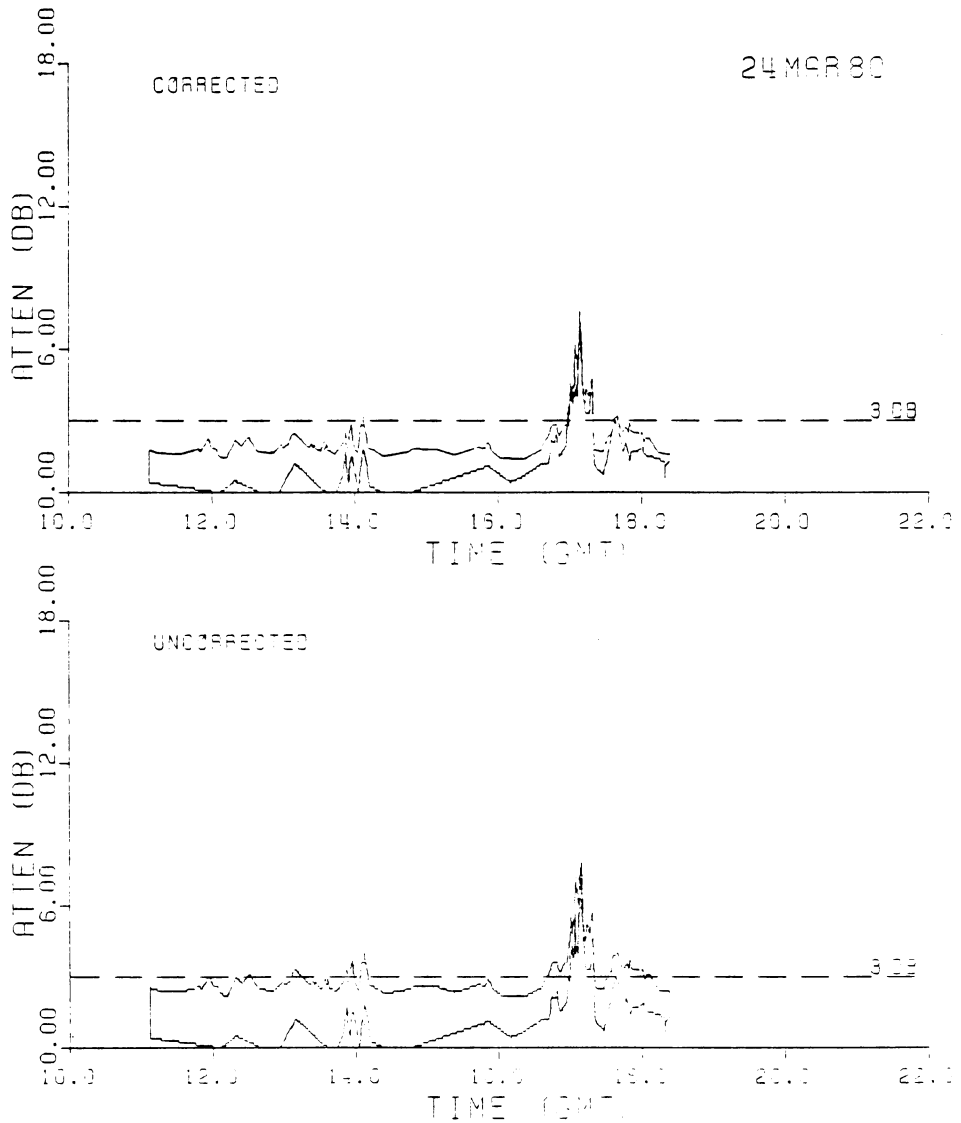


Figure 6.3-6 - Plot of Event on 24 March 1980.
 Bottom plot shows invalid radiometer
 attenuation (top line). Top plot shows
 corrected radiometer data again plotted
 with beacon attenuation.

Chapter VII

CONCLUSIONS

Analysis of two years of radiometric data has shown that the radiometer is a useful tool for predicting attenuation from sky noise temperatures. The radiometer used by the Satellite Communications Group predicted the attenuation at 11.6 GHz on a 10.7 degree slant path very well using a medium temperature of 265 K. Attenuations from 3 dB to 15 dB could be predicted which correlated well with SIRIO satellite beacon attenuation. An offset level of 0.4 dB added to the beacon level was desirable to account for the attenuation present due to the atmosphere in clear air conditions.

REFERENCES

1. Tiuri, M.E., [1964], 'Radio Astronomy Receivers', IEEE Transactions on Antennas and Propagation, Vol AP-12, pp. 930-938.
2. Kraus, J.D., [1966], Radio Astronomy, McGraw-Hill, New York, p. 244.
3. Dicke, R.H., [1946], 'The Measurement of Thermal Radiation at Microwave Frequencies', Review of Scientific Instruments Vol 17, pp. 268-275.
4. Orhaug, T. and W. Waltman, [1962], 'A Switched Load Radiometer', Publications of the National Radio Astronomy Observatory, Vol. 1, No. 12, pp. 179-204.
5. Evans, G. and C.W. McLeish, [1977], RF Radiometer Handbook, Artech House Inc., Dedham, MA.
6. Operating Manual, Type 2392C Universal Radiometer, AIL (Cutler-Hammer) Deer Park, Long Island, NY.
7. Smith, E.K. and J.W. Water, [1981], 'Microwave Attenuation and Brightness Temperature Due to Gaseous Atmosphere', NASA-JPL Publication No. 81-81.
8. Hall, M.P.M., [1975], Effects of the Troposphere on Radio Communications, IEE Publications, London, p. 75.
9. Thorn, R.W, J. Thirlwell, and D.J. Emerson, [1982], 'Slant Path Radiometer Measurements in the Range 11-30 GHz at Martlesham Heath England', British Telecommunications Memorandum No. R6/010/82.
10. Bell, R.R., [1977], 'Calibration of 20 and 30 GHz Radiometer By Using the ATS-6 Satellite Beacons', Electronics Letters, Vol. 13, No. 14, pp. 412-413.
11. Pratt, T. and D.J. Browning, [1977], 'Copolar Attenuation and Radiometer Measurements at 30 GHz for a Slant Path to Central England', Proceedings of the ATS-6 Meeting, Noordwijk.
12. Allnutt, J.E. and P.F. Shutie, [1977], 'Slant-Path Attenuation and Space-Diversity Results at 30 GHz

Using Radiometer and Satellite-Beacon Receivers',
Proceedings of the ATS-6 Meeting, Noordwijk.

13. Ippolito, L.J., [1971], 'Effects of Precipitation on 15.3 and 31.65 GHz Earth-Space Transmissions With the ATS-V Satellite', Proceedings of the IEEE, Vol. 59, No. 2, pp. 189-205.

**The vita has been removed from
the scanned document**